Archives of Pharmacal Research
https://doi.org/10.1007/s12272-026-01610-3

Online ISSN 1976-3786
Print ISSN 0253-6269

Archives of Pharmacal Research
www.springer.com/12272

RESEARCH ARTICLE

Tirzepatide mitigates atherosclerosis progression and modulates oxLDL-mediated proatherogenic effects in macrophages: evidence for M1/M2 homeostasis restoration

Mengjie Kang[1] · HaoLin Ren[2] · Yanru Zhen[1] · Limin Liu[3] · Qian Xu[1] · Yue Ma[1] · Lu Zhang[1] · Hui Jia[4] · Qing Chen[5] · Yuhan Jiang[6] · Junjia Gao[3] · Yueyang Liu[1] · Ming-Sheng Zhou[1]

Received: 7 August 2025 / Accepted: 21 March 2026

Abstract

Tirzepatide (TZP), a novel dual agonist of glucagon-like peptide (GLP)-1/glucose-dependent insulinotropic polypeptide (GIP) receptors (GLP-1R/GIPR), has been shown to reduce cardiovascular (CV) risk in patients with diabetes or obesity. This study investigated anti-atherosclerotic effects of TZP and the underlying mechanisms using apo $E^{-/-}$ mice and cultured macrophages. In the present study, apo $E^{-/-}$ mice were fed a high fat/high cholesterol (HF) diet with or without TZP treatment for 12 weeks. Atherosclerotic lesions, metabolic parameters, and M1/M2 macrophage homeostasis were assessed. In vitro, RAW264.7 and THP-1 macrophages were treated with oxLDL and TZP to evaluate foam cell formation, inflammation, and signaling pathways. The results showed that TZP significantly lowered body weight, plasma lipids, and atherosclerotic burden in vivo, and favorably modulated the expression of M1/M2 macrophage markers. ANCOVA suggested that the anti-atherosclerotic effect may be partially independent of metabolic improvements, although further studies are needed for confirmation. While these data support macrophage modulation as a key mechanism, other vascular cell types and plaque components likely contribute to the observed plaque-stabilizing effects. In vitro, TZP inhibited oxidized Low-density Lipoprotein (oxLDL)-induced cholesterol accumulation and foam cell formation, cluster of differentiation (CD) 36 expression and M1 inflammatory markers while promoting M2 markers. These effects were blocked by combined GLP-1R/GIPR antagonism and further confirmed in human THP-1 macrophages. Mechanistically, the anti-inflammatory effects and modulation of M1/M2 macrophage homeostasis by TZP were mediated via activating kruppel-like factor 4/the peroxisome proliferator-activated receptor γ pathway. Collectively, these findings indicate that TZP confers CV protection and anti-atherosclerotic benefits through both lipid-lowering dependent and independent mechanisms, highlighting its therapeutic potential for diabetic and obese patients who are at high risk of atherosclerotic CV diseases.

Keywords Atherosclerosis · Cardiovascular diseases · Glucagon-like peptide-1 · Insulinotropic polypeptide · Macrophage polarization

Mengjie Kang, HaoLin Ren and Yanru Zhen are equally contributed to this work.

✉ Junjia Gao
48026486@qq.com

✉ Yueyang Liu
yueyangliu1989@163.com

✉ Ming-Sheng Zhou
zhoums1963@163.com

[1] Shenyang Key Laboratory of Vascular Biology Institute, Science and Experimental Research Center, Shenyang Medical College, Huanghe N St. 146, Shenyang 110034, China

[2] Department of Radiology, The First Affiliated Hospital of Nanjing Medical University, Nanjing 21000, China

[3] Department of Cardiology, The 2nd Affiliated Hospital of Shenyang Medical College, Shenyang 110002, China

[4] School of Traditional Chinese Medicine, Shenyang Medical College, Shenyang 110034, China

[5] School of Pharmacy, Shenyang Medical College, Shenyang 110034, China

[6] School of the First Clinical Medicine, Shenyang Medical College, Shenyang 110034, China

Published online: 29 March 2026

Introduction

Global prevalence of obesity and type II diabetes (T2D), driven by sedentary lifestyle, urbanization, and diet changes, is on the rise, currently affecting more than 500 million adults worldwide (Chandrasekaran and Weiskirchen 2024). Both type II diabetes and obesity have become the most important risk factors for the development of cardiovascular (CV) diseases (CVDs), such as coronary atherosclerotic CVDs, myocardial infarction, stroke and heart failure (van Sloten et al. 2020; Park 2021; Kwan et al. 2023; Kufazvinei et al. 2024). Changes in metabolic profile such as hyperlipidemia and hyperglycemia are considered as the main drivers of T2D and obesity promoting CVDs (Chatzi et al. 2024; Chen et al. 2024). However, clinical studies have shown that intensive hypoglycemic therapies have not provided convincing evidence to reduce CV morbidity and mortality in patients with metabolic diseases at high CV risk, and recent studies from multiple large CV outcome trials (CVOTs) have demonstrated that some novel glucose-lowering agents such as glucagon-like peptide (GLP)-1 receptor (GLP-1R) agonists (GLP-1RA) and sodium-glucose co-transport 2 (SGLT2) inhibitors have great beneficial effects on reducing major adverse CV events and additional CV outcomes, which are largely independent of their hypoglycemic properties (Bilal et al. 2024; Kunutsor et al. 2024; Lalić et al. 2024). When choosing agents for treatment of metabolic diseases, clinicians should consider effects of these agents on CV system in addition to glucose-lowering effects, the novel hypoglycemic agents with CV beneficial effects, such as GLP-1RA, have recommended to treat metabolic diseases with high CV risk (Cersosimo et al. 2024; Katogiannis et al. 2024).

Tirzepatide (TZP) is a novel dual receptor agonist of glucose-dependent insulinotropic polypeptide (GIP) and GLP-1, offering significant advantages over GLP-1RA in glycemic control and weight management (Mather et al. 2024). Both GLP-1 and GIP are gut-derived hormones secreted by intestinal cells in response to food intake (Dinsmore et al. 2024). GLP-1 is produced by intestinal L cells, while GIP is released by intestinal K cells (Hammoud et al. 2024; Huang et al. 2024). GLP-1 activates GLP-1R on pancreatic islet b cells to regulate insulin release in a glucose-dependent manner, the activation of GLP-1R also slows down gastric emptying, suppresses glucagon secretion and appetite (Gilbert and Pratley 2020). Recent studies suggest that combining GLP-1R activation with other enteropancreatic hormones, such as GIP, enhances its metabolic efficacy. Evidence indicates that the combination of GLP-1 and GIP yields superior outcomes in managing body weight, reducing blood pressure, and mitigating inflammation compared with the use of selective GLP-1RAs alone (Regmi et al. 2024).

TZP has been approved for treatment of T2D and management of body weight in obese patients. In the SURPASS clinical trial, TZP demonstrated significantly reduction in glycated hemoglobin and body weight in T2D patients without increasing the risk of major CV events (Nicholls et al. 2024). Similarly, data from the SURMOUNT-1 randomized clinical trial showed that 72 weeks of TZP treatment improve cardiometabolic parameters, such as blood pressure and lipid profiles (Hankosky et al. 2024). These results suggest that TZP may offer CV benefits in addition to its robust metabolic effects, making it a promising candidate for the treatment of T2D patients with high CV risk factors. Despite these promising clinical results, there is a lack of preclinical evidence supporting CV effects of TZP. Given its potential for broad applications for treating obesity and T2D, particularly in the patients with high CV risk factors, further investigation into its CV effects is warranted (Bucheit et al. 2022; Dardano et al. 2024). Atherosclerotic CVDs, a chronic condition frequently associated with hyperlipidemia, T2D and obesity, remains common complication of these metabolic disorders (Ormazabal et al. 2018; Kassi et al. 2023). In this study, we investigated the role of TZP in preventing atherosclerotic CVDs in high-fat fed apo $E^{-/-}$ mice and elucidated underlying mechanisms.

Material and methods

Materials and reagents

TZP (CAS number: 2023788-19-2) was obtained from the Eli Lilly (Indiana, USA), the oxidized Low-density Lipoprotein (oxLDL) was purchased from the Yiyuan (Guangzhou, China), the H-89, GLP-1R antagonist 1, Kenpaullone and T0070907 were purchased from the MedChemExpress (New Jersey, USA) and the GIP (3-30) NH2 was acquired from PhoenixPeptide (Burlingame, California, USA). The primary antibodies were obtained from following companies: anti-cluster of differentiation (CD) 36, anti-Toll-like receptor 4 (TLR4), anti-P65 of nuclear factor kappa B (NFκB), anti-IκB and anti-p-IκB antibodies (Santa Cruz Biotechnology, Inc. TX, Dallas, USA), anti-ATP-binding cassette transporter (ABC) A1 and anti-phosphorated protein kinase A (p-PKA) antibodies (ImmunoWay, Inc. Suzhou, China), anti-ABCG1 antibodies (Abmart, Inc. Shanghai, China), anti-kruppel-like factor 4 (KLF4) antibody (Wanlei, Inc. Shenyang, China), anti-peroxisome proliferator-activated receptor γ (PPARγ), anti-arginase-1 (Arg-1), anti-F4/80 antibodies (Cell Signal Tech., Danvers, MA, USA), anti-inducible nitric oxide synthase (iNOS) (Abcam, Inc., Waltham, Massachusetts, USA), anti-CD86, anti-CD206, anti-glyceraldehyde 3-phosphate dehydrogenase (GAPDH) and horseradish peroxidase-conjugated secondary antibodies (ProteinTech

Group, Inc., Wuhan, China), Cy3-labeled goat anti-rabbit IgG (H + L) and FITC-labeled goat anti-mouse IgG (H + L) (Beyotime, Inc., Shanghai, China).

Animal protocols

Male 6-week-old apo $E^{-/-}$ mice were purchased from GemPharmatech Co., Ltd (Nanjing, China). All experimental protocols were implemented in compliance with the institutional guidelines for animal care and use and had been approved by the Animal Care and Use Committee of Shenyang Medical College (approval number: SYYXY2021032301, Shenyang, China). The mice were housed in a pathogen-free animal facility at Shenyang Medical College with free access to standard mouse chow and tap water. After one-week acclimation period, the mice were randomly assigned to one of four treatment groups for 12 weeks: Control group (Ctr): apo $E^{-/-}$ mice fed normal chow (17% caloric from fat, 0.03% cholesterol, 18% crude protein, 4% crude fiber, 5% crude ash), TZP group: apo $E^{-/-}$ mice fed normal chow with TZP treatment; HF group: apo $E^{-/-}$ mice fed high fat/high cholesterol diet (41% caloric from fat, 0.5% cholesterol, 19.47% casein, 4.99% corn starch, 9.98% maltodextrin, 33.76% sucrose, 4.99% cellulose, 0.99% corn oil, 19.97% anhydrous milk fat, Medicience Ltd. Yangzhou, China); HF + TZP group: apo $E^{-/-}$ mice fed a high-fat/high-cholesterol diet with TZP treatment. TZP was dissolved in water and administered through intraperitoneal injection at 10 nmol/kg twice a week, the other group was injected with the same volume of normal saline. Body weight was measured weekly, and fasting blood glucose levels were measured biweekly using an automatic blood glucometer (Roche Accu-CHEK Active, Mannheim, Germany). At the end of the study, the mice were fasted overnight, glucose tolerance test (GTT) was performed. Briefly, 20% glucose (1 g/kg) was injected intraperitoneally, blood glucose levels were measured at 0 (pre-injection), 15, 30, 60, 90 and 120 min after the injection using the glucometer. The mice were then anesthetized with a mixture of 100 mg/kg ketamine and 20 mg/kg xylazine, blood was collected from the eyeball. The abdomen and chest were opened, and all abdominal fat was excised and weighed. The entire aorta was isolated for the assessment of atherosclerotic lesion and histological analysis.

Quantitative atherogenic lesion areas and histological analysis

The entire aorta (from the aortic arch to iliac bifurcation) was carefully excised and rinsed with phosphate buffered saline (PBS). Periadventitial tissue was meticulously removed. Entire aorta was then opened longitudinally along the ventral edge to expose the intimal surface, and lipids were stained using Oil Red O. The images of stained aorta were captured with a Canon digital camera. Atherosclerotic lesions were identified on the digital image. For both the aortic lesion area and the aortic sinus morphological analyses described below, quantifications were performed in a blinded manner. Lesion area including, entire aorta and specific segments such as aortic arch, thoracic and abdominal aorta, were quantified using ImageJ software (version 2.1.0/1.53c), results were expressed as percentage of lesion area relative to the total observed area.

For histological analysis of lesion formation in the aortic sinus, a small segment of aortic tissue (from the heart valve to the aortic arch) was taken and frozen in OCT reagent. Series of cryosections with 5 mm thickness were cut from the beginning of the aortic valve leaflets to the aortic sinus. The section was stained with Oil Red O to visualize lipid deposition. Images were acquired with a Leica DM4B fluorescence microscope (Leica Microsystems Inc., Journal Pre-proof Mannheim, Germany). Average lesion areas, represented by positively Oil Red O staining areas, were quantitated using digital images from 6 serial sections per aortic sinus sample, and the measurements were analyzed using ImageJ 2.1.0/1.53c software.

For detailed plaque characterization, serial sections adjacent to those used for Oil Red O staining were subjected to Hematoxylin and Eosin (H&E) and Masson's Trichrome staining. H&E staining was performed according to standard protocols to visualize general plaque morphology and to identify the necrotic core, characterized by areas of acellular, eosinophilic debris. Masson's Trichrome staining was used to delineate collagen fibers, which appear blue, thereby allowing for the quantification of the fibrous cap within the plaques. All stained sections were imaged under a light microscope. Morphometric analyses of the plaque necrotic core area from H&E-stained sections and the fibrous cap area from Masson's Trichrome-stained sections were performed blindly using ImageJ software (version 2.1.0/1.53c). The results for the necrotic core were expressed as a percentage of the total plaque area, and the fibrous cap thickness was measured at its thinnest point across multiple serial sections per sample.

Biochemistry analysis

Plasma levels of total cholesterol (TC) and total triglyceride (TG) were determined using a TC assay kit (TC: A111-1-1; Nanjing Jiancheng Bioengineering Institute Co., Nanjing, China) and a TG assay kit (TG: A110-1-1; Nanjing Jiancheng Bioengineering Institute Co., Nanjing, China), respectively, according to the manufacturer's instructions. Plasma sample (2.5 mL) was diluted appropriately and added to each well of a 96-well plate; followed by the addition of 250 μL working solution. The plate was incubated at 37 °C for 10 min, and the absorbance was measured at

500 nm wavelength. Plasma TG and TC concentrations were calculated based on a standard concentration curve fit. For the determination of cellular cholesterol contents, macrophages were incubated in six-well dishes in the presence or absence of oxLDL (50 mg/mL) or TZP (100 nmol/mL) for 24 h. Total cellular cholesterol was extracted by adding 1 mL hexane/isopropanol (3:2, v/v) to each well. The solvent was then evaporated, and residue was dissolved in ethanol. Cholesterol content was determined using the same procedure as described for plasma cholesterol.

Immunofluorescence analysis

A piece of aortic tissue (aortic arch) was frozen in OCT-reagent and cryosectioned into 5 μm thick slices. Then, the sections were heated in a 60 °C water bath for 1 h to facilitate antigen exposure. The section was incubated overnight with primary antibodies against CD86 (13395-1-AP, ProteinTech, Wuhan, China; 1:400), CD206 (81525-1-RR, ProteinTech, Wuhan, China; 1:200), iNOS (ab178945, Abcam, Waltham, Massachusetts, USA; 1:200), Arg-1 (#93668, Cell Signal Tech., Danvers, MA, USA; 1:200), F4/80 (sc-377009, Santa Cruz, Dallas, TX, USA; 1:200), KLF4 (WL02532, Wanlei, Shenyang, China; 1:200) and p65 of NF*k*B (#8242, Cell Signal Tech., Danvers, MA, USA; 1:200) at 4 °C overnight. After three washes with PBS, the sections were incubated with fluorescent-conjugated secondary antibodies (Cy3 or FITC, Beyotime, Shanghai, China; 1:500) at room temperature for 1 h. Nuclei were counterstained with DAPI. Fluorescent images were acquired with Leica DM4B fluorescence microscope (Leica Microsystems Inc., Journal Pre-proof Mannheim, Germany), fluorescence intensity was quantified using digital images obtained from 6 serial sections per sample using ImageJ 2.1.0/1.53c software.

Cell culture

Murine macrophage RAW264.7 cells were cultured in high-glucose DMEM (25 mmol/L) medium (Cytiva, USA) supplemented with 10% fetal bovine serum (FBS, YOSHI, Wuhan, China) and the 1% penicillin–streptomycin antibiotics (Solarbio, Beijing, China) at 37 °C and 5% CO_2. Cells between passages 4–16 were used for experiments. Cells were seeded in six-well plates and serum-starved in DMEM medium without FBS for 24 h before the experiments were conducted. For M1/M2 macrophage homeostasis studies, cells were treated with control (culture medium), oxLDL (50 mg/mL), TZP (100 nmol/mL) or a combination of oxLDL and TZP for 24 h, cells then were harvested for analysis by Real-time PCR or Western blotting. In specific experiments, cells were preincubated with a PPARγ inhibitor (100 nmol/L), p-PKA inhibitor (5 μmol/L) or the KLF4 inhibitor kenpaullone (2 μmol/L) for 30 min before the incubation with oxLDL and TZP. Additionally, the effect of TZP on M1/M2 macrophage markers was further validated in human THP-1-derived macrophages.

Foam cell formation

Murine RAW264.7 macrophages or human THP-1/macrophages were cultured on chamber slides and pretreated with varying concentrations of TZP (10, 20, 50 and 100 nmol/L) for 30 min, followed by the incubation with oxLDL (50 mg/mL) for 72 h. THP-1 cells were selected as a human macrophage model due to their well-characterized differentiation protocols, genetic homogeneity enabling reproducible mechanistic studies, and extensive validation in atherosclerosis research (Chanput et al. 2014). Subsequently, the cells were stained with Oil Red O to visualize lipid deposits, and nuclei was stained with hematoxylin to facilitate cell identification. The images were obtained with a light microscope. The extent of lipid deposition in foam cells was quantified by measuring the Oil Red O positively stained areas relative to the total cell area.

Western blotting

The RAW264.7 cells were harvested and homogenized using RIPA buffer containing protease cocktail. Protein concentration was determined using a BCA assay kit (P0012; Beyotime, Shanghai, China) according to the manufacturer's instructions. A total of 60 mg of protein from the supernatant was separated in an 8% SDS-PAGE gel and transferred to PVDF membranes. The membranes were blocked with a 5% BSA blocking solution at room temperature for 2 h. Then, the membranes were overnight incubated with primary antibodies, including anti-CD36 (sc-7309; Santa Cruz Biotech, Dallas, TX, USA; 1:100), anti-p-PKA (YP0226; Immunoway, CA, USA; 1:1000), anti-ABCA1 (YN2847; Immunoway, CA, USA; 1:500), anti-ABCG1 (PA2410; Abmart, Shanghai, China; 1:1000), anti-TLR4 (sc-293072; Santa Cruz, Dallas, TX, USA; 1:500), anti-pIκB-α (sc-8404; Santa Cruz, Dallas, TX, USA; 1:500), anti-IκB-α (sc-1643; Santa Cruz, Dallas, TX, USA; 1:500), anti-PPARγ (#2435; Cell Signal Tech., Danvers, MA, USA; 1:1000), anti-KLF4 (WL02532; Wanlei, Shenyang, China; 1:1000) and anti-GAPDH (60004-1-IG; ProteinTech, Wuhan, China; 1:5000) antibodies at 4 °C overnight. After three washes with TBST, the membranes were incubated with horseradish peroxidase-conjugated secondary antibodies (SA00001-2 or SA00001-1; ProteinTech, Wuhan, China) for 1 h at room temperature. The immunoblots were visualized by enhanced chemiluminescence (P10300; NCM Biotech, Suzhou, China), and detected by an Aplegen Omega Lum G Gel Documentation System (Aplegen Inc., Pleasanton), the protein expression was quantified by densitometric analyses with ImageJ

2.1.0/1.53c software system. The data was normalized by housekeeping protein GAPDH and expressed as fold changes relative to the control group.

KLF4 gene silencing

KLF4 gene silencing was performed in murine RAW264.7 macrophages using synthetic siRNA KLF4 (RiboBio Co., Ltd.; Guangzhou, China), a non-targeting scrambled siRNA sequence (si-NC) was used as negative control. For transfection, cells were seeded into culture plates and allowed to reach 60–70% confluence. The siRNA-lipid complexes were prepared by incubating the respective KLF4 siRNA or si-NC with Lipofectamine 3000 transfection reagent in Opti-MEM reduced serum medium, according to the manufacturer's instructions. This complex was then added to the cells. After an incubation of 6–8 h, the transfection mixture was replaced with fresh complete medium. The cells were harvested 48 to 72 h post-transfection. The efficiency of KLF4 gene silencing was validated by Western blot analysis with approximately 70% reduction in KLF4 protein expression.

Real-time PCR

Total RNA was extracted using the TaKaRa MiniBEST Universal RNA Extraction Kit (#9767; Takara, Kusatsu, Japan) according to the manufacturer's instructions. Subsequently, 2 μg of total RNA was reverse-transcribed into cDNA using the HiScript IV RT SuperMix (Vazyme Nanjing, China) according to the manufacturer's instructions. Real-time PCR was performed to quantify the expression of target genes, including GLP-1R, GIPR, tumor necrosis factor (TNF)α, C–C motif ligand (CCL)2, TLR4, interleukin (IL)-6, Arg-1, IL-10 and GAPDH. The reaction was carried out in a total volume of 20 μL containing 100 ng of sample cDNA solution, 0.1 mmol/L reverse and forward primers, and SYBR qPCR Master Mix (Vazyme, Nanjing, China) using the LineGene 9600 Plus PCR System (Bioer technology, Hangzhou, China). The relative mRNA expressions were normalized to a housekeeping gene GAPDH, and expressed as fold change vs. control group. The sequences of reverse and forward primers used for each target genes are listed in Table 1.

RNA extraction, library construction and sequencing

Total RNA was extracted from the macrophages using Trizol reagent kit (Vazyme, Nanjing, China) following the manufacturer's protocols. RNA quality was assessed using an Agilent 2100 Bioanalyzer (Agilent Tech., Palo Alto, CA) and RNase-free agarose gel electrophoresis, with all samples meeting the quality threshold of RNA Integrity Number (RIN) > 8.0. Library construction was performed using the Illumina TruSeq Stranded mRNA LT Sample Prep Kit. mRNA was enriched by mRNA Capture Beads, and ribosomal RNA (rRNA) was removed using the Ribo ZeroTM magnetic assay kit (Epicenter, Madison, WI). The enriched mRNA was fragmented into short fragments and reverse-transcribed into cDNA. Followed by second-strand cDNA synthesis. The cDNA fragments were purified with QiaQuick PCR extraction kit (Qiagen, Venlo, The Netherlands), followed end repaired and poly (A) addition, and ligated with Illumina sequencing adapters.

The ligation products were size-selected using agarose gel electrophoresis, amplified by PCR, and subjected to sequencing on the Illumina NovaSeq X Plus platform (Gene Denovo Biotechnology Co., Guangzhou, China). Raw sequencing reads were quality-controlled using Fastp (version 0.18.0) with following criteria: (1) removing reads containing adapters; (2) exclusion of reads > 10% of unknown nucleotides(N); (3) filtering low quality reads where more than 50% of bases had a Q-value ≤ 20. The resulting high-quality clean reads were aligned to the reference genome (GRCm38) using HISAT2 (version 2.1.0) with default parameters. Gene expression quantification was performed using StringTie (version 1.3.1) and RSEM software, with normalization conducted using the transcripts per kilobase million (TPM) method.

Differential expression analysis was carried out with DESeq2, applying a threshold of false discovery rate (FDR) < 0.05 and absolute $\log_2$ fold change ≥ 1. Gene

Table 1 the premier sequences for target genes

Gene name	Forward primer sequences	Reverse primer sequences
GLP-1R	CTCCGAGCACTGTCCGTCTT	GATAACGAACAGCAGCGGAAC
GIPR	CTACTCCCTGTCCCTGACGA	AGCTGATCTCGGGTGAGGAT
TNFα	TCTTCTCATTCCTGCTTGTGG	ATGAGAGGGAGGCCATTTG
CCL2	TGCTCTGTGAAGGGAATGGGTGTT	AGTCCTTGATGGTGGTGCATGAGA
TLR4	AAATGCACTGAGCTTTAGTGGT	TGGCACTCATAATGATGGCAC
IL-6	TGGCCTTCCGTGTTCCTAC	GAGTTGCTGTTGAAGTCGCA
Arg-1	CTTGCGAGACGTAGACCCTG	TCCATCACCTTGCCAATCCC
IL-10	GCTCTTACTGACTGGCATGAG	CGCAGCTCTAGGAGCATGTG
GAPDH	CTTTGGTATCGTGGAAGGACTC	GTAGAGGCAGGGATGATGTTCT

abundance analysis, pathway enrichment analysis and differential function Gene Ontology (GO) enrichment analysis were performed using cluster Profiler, with significance defined as Bonferroni-corrected p-value < 0.05.

Statistics

All data are expressed as the mean ± SEM of individual animal or cell-based experiments. A priori power analysis was performed using G*Power software (version 3.1.9.7) based on pilot data of atherosclerotic lesion area in apo $E^{-/-}$ mice. Assuming an effect size (Cohen's d) of 1.5, $\alpha = 0.05$, and power = 0.80, the minimum required sample size was calculated to be five animals per group. For in vitro experiments, based on preliminary data for macrophage polarization markers, three independent experiments were determined to provide 80% power to detect a two-fold difference at $\alpha = 0.05$. For newly performed validation experiments during revision, a sample size of n = 5 was used to enhance statistical robustness.

Statistically significant differences among multiple groups were evaluated by one-way ANOVA with Tukey's multiple comparisons test using GraphPad Prism 8 software. To specifically assess the treatment effect of TZP on atherosclerotic lesion area independent of changes in body weight and plasma lipids, an analysis of covariance (ANCOVA) was performed with final body weight and total cholesterol level as covariates. Effect sizes with corresponding 95% confidence intervals were calculated and reported for all outcomes (supplement Table 1). A p value of less than 0.05 was considered statistically significant.

Exclusion criteria were predefined as follows: (1) animals that did not complete the treatment period due to non-treatment-related illness or death; (2) samples with technical artifacts precluding reliable quantification; and (3) statistical outliers identified using Grubbs' test ($\alpha = 0.05$) with documented technical justification. No samples met these exclusion criteria in the present study.

Results

TZP inhibits body weight gain and improves metabolic profiles in apo $E^{-/-}$ mice

A schematic diagram of the experimental protocols is shown in Fig. 1A. HF diet intake for 12 weeks significantly increased body weight (Fig. 1B, C), abdominal fat weight (Fig. 1B, D), plasma levels of TG (Fig. 1E) and TC (Fig. 1F) in apo $E^{-/-}$ mice. HF diet increased fasting blood level of glucose (Fig. 1G) and impaired glucose tolerance (Fig. 1H) compared with apo $E^{-/-}$ mice fed a normal mouse chow. Treatment with TZP significantly lowered plasma lipid levels in apo $E^{-/-}$ mice fed either a normal or HF diet (Fig. 1E, F, all $p < 0.05$). Moreover, TZP significantly mitigated body weight gain, reduced abdominal fat weight and fasting blood level of glucose and improved glucose tolerance in apo $E^{-/-}$ mice on a HF diet but not those on a normal mouse chow (Fig. 1B–D, G, H, all $p < 0.05$). These results suggest that TZP improves metabolic profile in apo $E^{-/-}$ mice, especially in HF/apo $E^{-/-}$ mice.

TZP inhibits atherosclerotic lesion formation in apo $E^{-/-}$ mice

To evaluate the effect of TZP on atherosclerotic lesion formation, we measured intimal lipid accumulation and atheromatous lesion areas on isolated aortas from the arch to the iliac bifurcation of aorta stained with Oil Red O. The staining revealed that extensive atherosclerotic plaque formation throughout the entire aorta of apo $E^{-/-}$ mice subjected to HF diet, total lesion areas of the enface aorta as well as segmental lesion areas in the aortic arch, thoracic aortas and abdominal aortas, were significantly increased in apo $E^{-/-}$ mice fed a HF diet as compared to those on a normal mouse chow (Fig. 2A, B, all $p < 0.05$). TZP treatment significantly reduced total lesion areas in the aorta (− 40.1%, 95% CI 1.691 to 15.800) and segmental lesion areas of aortic arch, thoracic and abdominal aortas (Fig. 2A, B, all $p < 0.05$) in HF/apo $E^{-/-}$ mice. To explore whether this atheroprotective effect might be independent of the concomitant reductions in body weight and plasma cholesterol, an ANCOVA was performed. The results showed that the reduction in atherosclerotic lesion area by TZP remained statistically significant (Fig S1A & B, Tables S2 and S3, all $p < 0.05$) after adjusting for final body weight and total cholesterol levels, suggesting a potential direct anti-atherosclerotic effect beyond its systemic metabolic improvements. However, we acknowledge that this statistical approach cannot definitively establish independence, and these findings should be interpreted with caution.

We further performed histological analysis of aortic sinus lesions and lipid deposition using Oil Red O and H&E staining. Given its established role as the gold-standard site for assessing atherosclerotic lesion severity and complexity in murine models (Burnett et al. 2004), the aortic sinus was selected for analysis. The lesion areas and lipid deposition were significantly increased in the aortic sinus section of HF/apo $E^{-/-}$ mice, which were significantly reduced in HF/apo $E^{-/-}$ mice treated with TZP (Fig. 2C–F, − 25.8% for lesion areas, 95% CI 1.788 to 13.960; and − 27.4% for lipid deposition, 95% CI 1.707 to 16.900; $p < 0.05$). Furthermore, quantitative analysis of H&E and Masson's Trichrome-stained sections revealed a markedly increased necrotic core area and a decreased fibrous cap area within the plaques of HF/apo $E^{-/-}$ mice, indicating a vulnerable plaque phenotype.

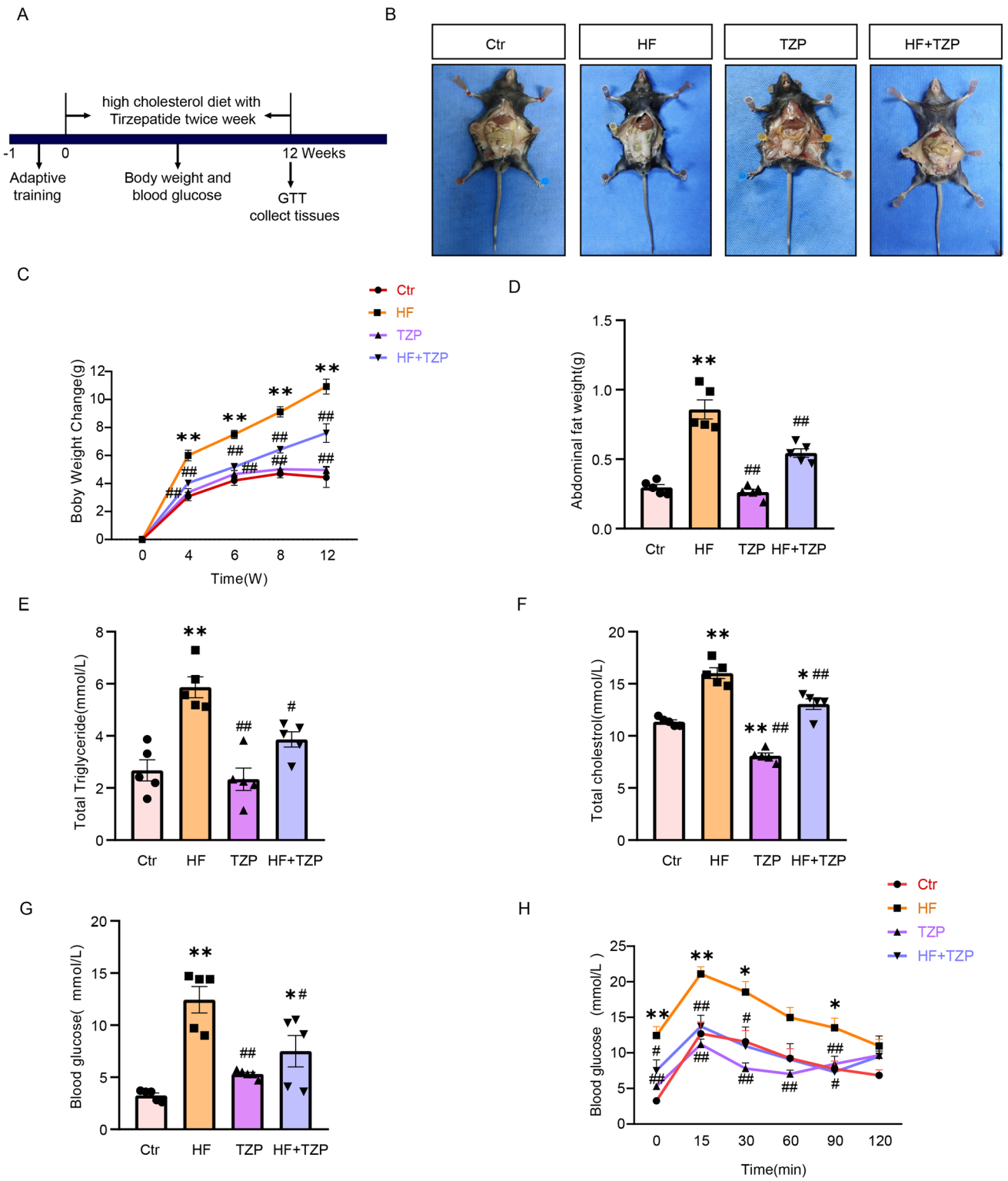

Fig. 1 Effects of tirzepatide (TZP) on body weight and metabolic parameters in atherogenic apo $E^{-/-}$ mice. **A** In vivo flow chart. **B** Representative photograph showing abdominal fat accumulation. **C** Body weight gain over 12 weeks of treatment. **D** Abdominal fat weight. **E** Total fasting plasma triglyceride level. **F** Total fasting plasma cholesterol level. **G** Fasting blood glucose level. **H** Glucose tolerance. Experimental groups include apo $E^{-/-}$ mice fed a normal mouse diet (Ctr), apo $E^{-/-}$ mice fed a high-fat/high-cholesterol diet (HF), apo $E^{-/-}$ mice on a normal mouse diet with TZP treatment (TZP), and apo $E^{-/-}$ mice on an HF diet with TZP treatment (HF + TZP). Data are expressed as mean ± SEM. $^{*}p < 0.05$ vs. Ctr group; $^{**}p < 0.01$ vs. Ctr group; $^{\#}p < 0.05$ vs. HF group; $^{\#\#}p < 0.01$ vs. HF group; N = 5

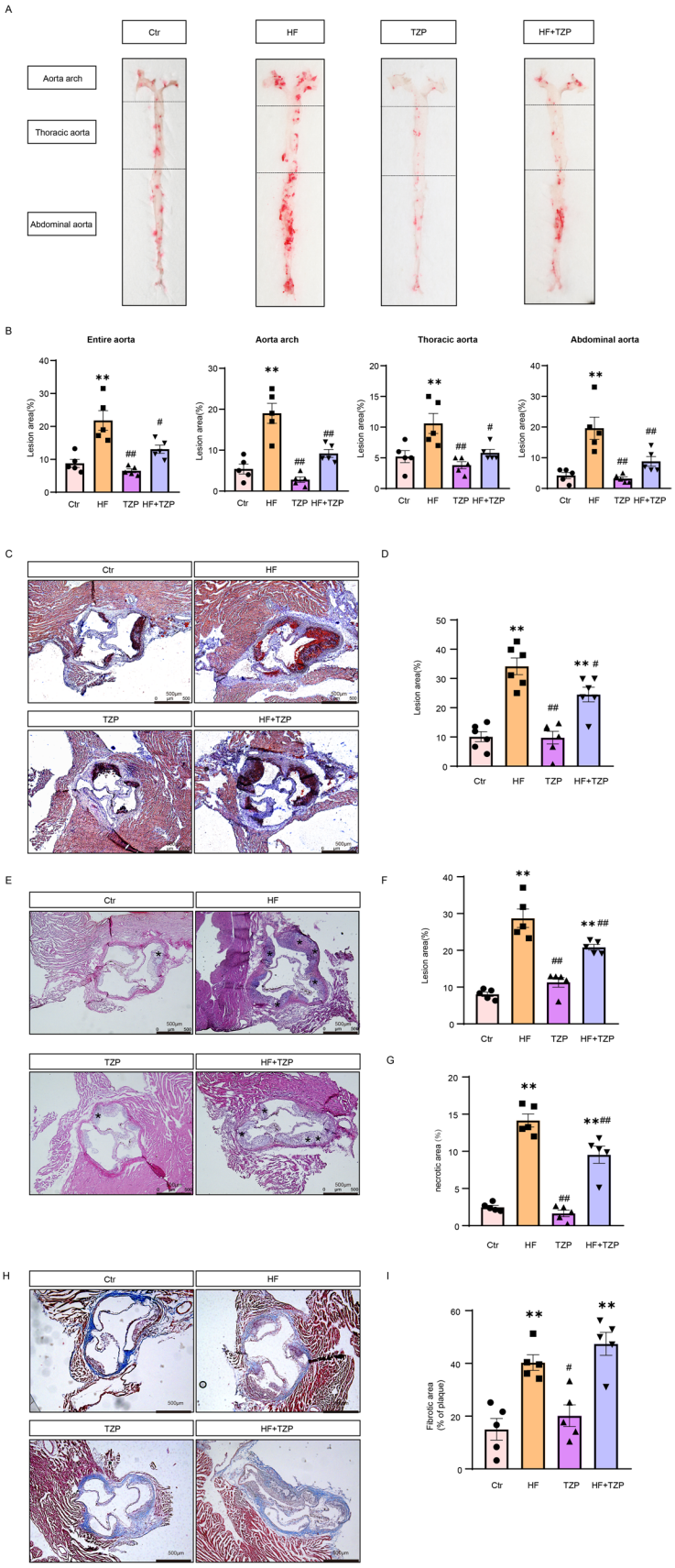

Fig. 2 TZP treatment reduces atherosclerotic plaque formation in apo $E^{-/-}$ mice. **A** and **B** Morphometric analysis of aortic lesion areas. **A** Representative photographs of enface aortas from apo $E^{-/-}$ mice. **B** Quantitation of lesion areas in whole aortas, the aortic arch, thoracic aorta, and abdominal aorta. **C**–**F** Histological analysis of aortic sinus lesion areas. Representative images (**C**) and quantitation (**D**) of atherosclerotic lesions stained with Oil Red O. Representative images (**E**) and quantitation (**F**) of atherosclerotic lesions stained with hematoxylin and eosin (**H** and **E**). Data are expressed as mean ± SEM. $^{*}p < 0.05$ vs. Ctr group; $^{**}p < 0.01$ vs. Ctr group; $^{\#}p < 0.05$ vs. HF group; $^{\#\#}p < 0.01$ vs. HF group; N = 5; Scale bar = 500 mm

Importantly, TZP treatment significantly reversed these changes by reducing the necrotic core (− 32.5%, 95% CI 1.504 to 7.712; Fig. 2G–I). These findings suggest that TZP not only reduces plaque burden but also promotes plaque stability.

TZP modulates macrophage infiltration and promotes a phenotypic shift from M1 to M2 in plaques of HF/apo $E^{-/-}$ mice

Macrophages play a critical role in the initiation and progression of vascular inflammation and atherosclerotic lesion development (Groh et al. 2018). The balance between pro-inflammatory M1 and anti-inflammatory M2 macrophage phenotypes critically influences plaque stability (Gianopoulos et al. 2025). We first assessed this balance in the aortic sinus by immunofluorescence staining for the M1 marker CD86 and the M2 marker CD206 (Paul et al. 2019; Liu et al. 2020). Compared to apo $E^{-/-}$ mice on a normal diet, HF/apo $E^{-/-}$ mice exhibited a significant increase in CD86 fluorescence intensity alongside a marked decrease in CD206 intensity (Fig. 3A–D, all $p < 0.05$). TZP treatment had no effect on these markers in mice on a normal diet. However, in HF/apo $E^{-/-}$ mice, TZP significantly attenuated the HF-induced increase in CD86 and restored the level of CD206 (Fig. 3A–D, all $p < 0.05$).

To further validate this M1/M2 macrophage homeostasis, we performed immunofluorescence co-staining using the pan-macrophage marker F4/80 together with the classic M1 marker iNOS and the M2 marker Arg-1. This analysis revealed that TZP treatment significantly reduced the population of $F4/80^+$ alone (− 48.1%, 95% CI 48.880 to 85.670) and $F4/80^+/iNOS^+$ double-positive (M1) macrophages while concurrently increasing the population of $F4/80^+/Arg\text{-}1^+$ double-positive (M2) macrophages within the atherosclerotic lesions (Fig. 3E–I, all $p < 0.05$). These findings suggest that TZP promotes a more stable plaque phenotype, which is consistent with the observed shift toward M2 macrophage polarization. However, other cell types and matrix components not assessed in this study may also contribute to these stability changes. Collectively, these data demonstrate that TZP favorably modulates the M1/M2 macrophage homeostasis in the atherosclerotic vascular wall, suppressing the pro-inflammatory M1 state and promoting the anti-inflammatory M2 state, thereby helping to restore macrophage homeostasis.

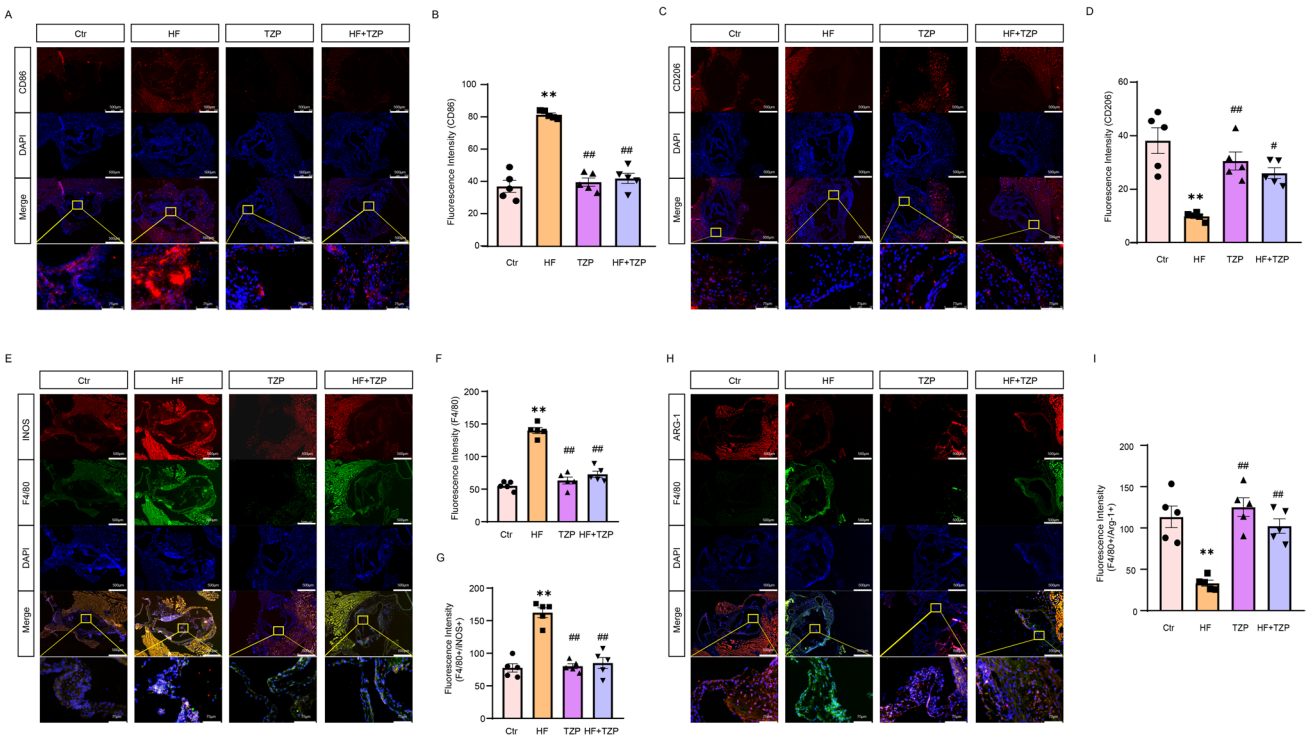

Fig. 3 TZP modulates M1/M2 macrophage homeostasis in atherogenic apo $E^{-/-}$ mice. Representative immunofluorescence images of the M1 marker cluster of differentiation (CD)86 (**A**) and the M2 marker CD206 (**C**), and their correspondence fluorescence quantitation (B&D). Representative immunofluorescence double-staining images of F4/80 with M1 marker inducible nitric oxide synthase (iNOS) (**E**) and M2 marker arginase-1 (Arg-1, **H**), and fluorescence quantitation of F4/80 (**F**), F4/80 with iNOS (**G**) or with Arg-1 (**I**). Data are expressed as mean ± SEM. $^{*}p < 0.05$ vs. Ctr group; $^{**}p < 0.01$ vs. Ctr group; $^{\#}p < 0.05$ vs. HF group; $^{\#\#}p < 0.01$ vs. HF group; N = 5; Scale bar = 250 mm or 75 mm

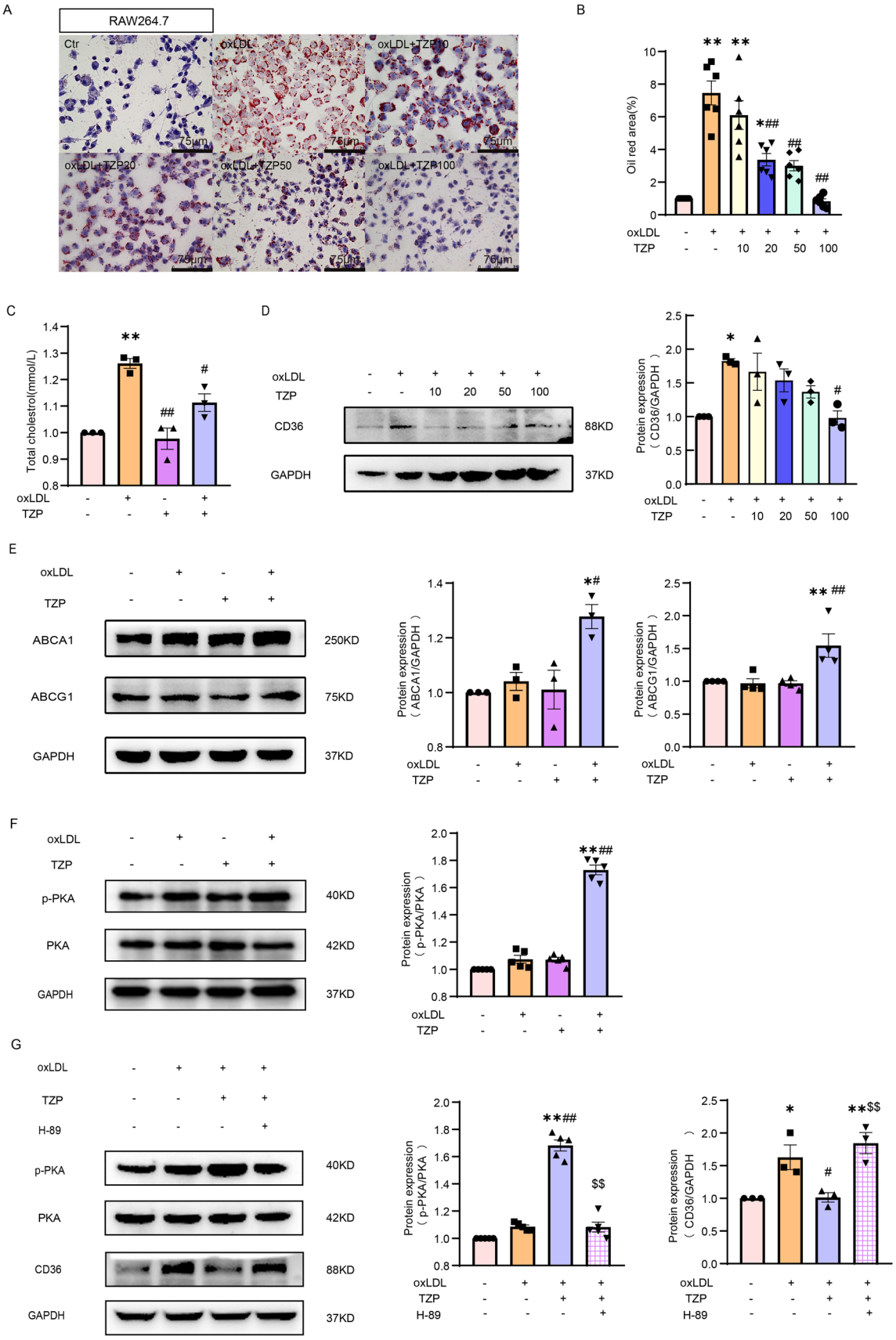
A
RAW264.7
Ctr
oxLDL
oxLDL+TZP10
oxLDL+TZP20
oxLDL+TZP50
oxLDL+TZP100
75μm
B
Oil red area(%)
oxLDL
TZP
C
Total cholestrol(mmol/L)
D
CD36
GAPDH
88KD
37KD
Protein expression (CD36/GAPDH)
E
ABCA1
ABCG1
250KD
75KD
Protein expression (ABCA1/GAPDH)
Protein expression (ABCG1/GAPDH)
F
p-PKA
PKA
40KD
42KD
Protein expression (p-PKA/PKA)
G
H-89
Protein expression (CD36/GAPDH)

◂**Fig. 4** TZP inhibits oxLDL-induced foam cell formation in RAW267.4 macrophages. **A** Representative images of lipid deposition and foam cell formation stained with Oil Red O, and **B** its quantitation. **C** Intracellular cholesterol content quantified using a cholesterol assay kit. **D** Protein expression of CD36; **E** ATP-binding cassette transporter (ABC) A1 and ABCG1; **F** phosphorated protein kinase A (p-PKA). **G** Representative image bands and their quantitation of CD36 and p-PKA protein expression following PKA inhibitor H-89 treatment. Data are expressed as mean ± SEM. Experimental groups include control RAW264.7 cells (Ctr), RAW264.7 cells treated with oxidized Low-density Lipoprotein (oxLDL), RAW264.7 cells with oxLDL and TZP treatment (oxLDL + TZP). $^{*}p < 0.05$ vs. Ctr group; $^{**}p < 0.01$ vs. Ctr group; $^{\#}p < 0.05$ vs. oxLDL group; $^{\#\#}p < 0.01$ vs. oxLDL group; $^{\$}p < 0.05$ vs. oxLDL + TZP group; $^{\$\$}p < 0.01$ vs. oxLDL + TZP group; N = 3; Scale bar = 75 mm

TZP inhibits oxLDL-induced CD36 expression and foam cell formation in cultured macrophages

Excessive cholesterol deposition in macrophages, leading to foam cells, is a key pathological step in the development and progression of atherosclerosis (Wang et al. 2022). Our in vivo studies have demonstrated that TZP significantly inhibits lipid deposition and atherosclerotic lesion formation. We determined foam cell formation using Oil Red O staining, and intracellular cholesterol contents were measured using a cholesterol assay kit. Consistent with the in vivo findings in apo $E^{-/-}$ mice, TZP reduced oxLDL-induced foam cell formation in both murine RAW264.7 (− 88.8%, 95% CI 4.423 to 8.836, Fig. 4A, B) and human THP-1 macrophages (Fig S2A & B, all $p < 0.05$) and intracellular cholesterol content (Fig. 4C, $p < 0.05$). Intracellular cholesterol homeostasis depends on the balance between cholesterol uptake and efflux, CD36 is a key receptor mediating oxLDL uptake, while ABCA1 and ABCG1 are essential transporters facilitating cholesterol efflux. Exposure to oxLDL significantly increased the protein expression of CD36, and TZP inhibited oxLDL-induced CD36 expression in dose-dependent manner (Fig. 4D, $p < 0.05$). oxLDL did not significantly affect the expression of ABCA1 and ABCG1, nor TZP alone. However, TZP in the presence of oxLDL significantly increased the expression of ABCA1 and ABCG1 (Fig. 4E, $p < 0.05$). Both GLP-1 and GIP receptors are G-protein-coupled receptor, the activation of these receptors induces PKA phosphorylation. As shown in Fig. 4F, TZP in the presence of oxLDL increased p-PKA, and treatment with PKA inhibitor H-89 prevented TZP downregulation of CD36 expression (Fig. 4G, $p < 0.05$). Therefore, TZP downregulates CD36 through stimulating p-PKA. Given the critical role of CD36 in regulating macrophage uptake of oxLDL, TZP's inhibition of foam cell formation and intracellular cholesterol accumulation may be partially attributed to its downregulation of CD36.

TZP inhibits oxLDL-induced macrophage inflammation and promotes M1/M2 macrophage homeostasis in cultured macrophages

To investigate the mechanisms underlying anti-atherosclerotic effects of TZP, we performed a broad-spectrum screening in oxLDL-treated murine macrophages using RNA-seq analysis. Differential RNA expression analysis revealed that TZP in the presence of oxLDL upregulated the expression of 38 genes and downregulated the expression of 43 genes compared to macrophages treated with oxLDL alone (Fig. 5A). Among the top 20 genes affected by TZP, 10 genes were associated with the regulation of macrophage inflammation and atherosclerosis, including Il12rb1, Rgcc, Apba1, Cavin1, Cd5l, Alc39a10, Dcn, Fn1, Sparc, Lox (Fig. 5B). GO enrichment analysis showed that TZP affected top 20 major signaling pathways involved in atherosclerotic plaque development. These pathways included extracellular matrix structural constituent, extracellular matrix, movement of cell or subcellular component, collagen-containing extracellular matrix, fibrinogen complex. The pathway analysis using Selective Kyoto Encyclopedia of Genes and Genomes (KEGG) highlighted TZP's effects on the pathways involved in macrophage regulation and inflammatory process. These pathways include Rheumatoid arthritis, IL-17 signaling pathway, tissue growth factor (TGF)-beta signaling pathway, TNF signaling pathway, chemokine signaling pathway, Th1 and Th2 cell differentiation, extracellular matrix (ECM)-receptor interaction, viral protein interaction with cytokine and cytokine receptor, cytokine-cytokine receptor interaction (Fig. 5C).

To further assess signaling pathway alterations affected by TZP, Gene Set Enrichment Analysis (GSEA) analysis was performed, and the results showed that TZP upregulated epoxygenase P450 pathway while downregulating the process on membrane disruption, CCR6 chemokine receptor binding, trace-amine receptor activity, histidine metabolism and glycosaminoglycan (Fig. 5D, $p < 0.05$). These results indicate that TZP exerts remarkable regulatory effects on macrophage inflammation. Based on RNA-seq results, we further investigated effect of TZP on M1/M2 macrophage homeostasis. TZP significantly inhibited oxLDL-induced increase in the expression of M1 inflammatory genes TNFα, CCL2 and IL-6 and reversed the decrease in the expression of M2 anti-inflammatory genes IL-10 and Arg-1 (Fig. 6C, all $p < 0.05$). Consistent with the findings in murine macrophages, TZP treatment in THP-1-derived macrophages also confirmed the suppression of M1 inflammatory cytokines (TNF-α, IL-6, and TLR4) (Figs S3, all $p < 0.05$). It has been shown that oxLDL induces macrophage activation through TLR4/nuclear factor kappa B (NFκB) inflammatory pathway, TZP significantly inhibited oxLDL-upregulation the expression of TLR4 and phosphorylation of I*k*B (ratio

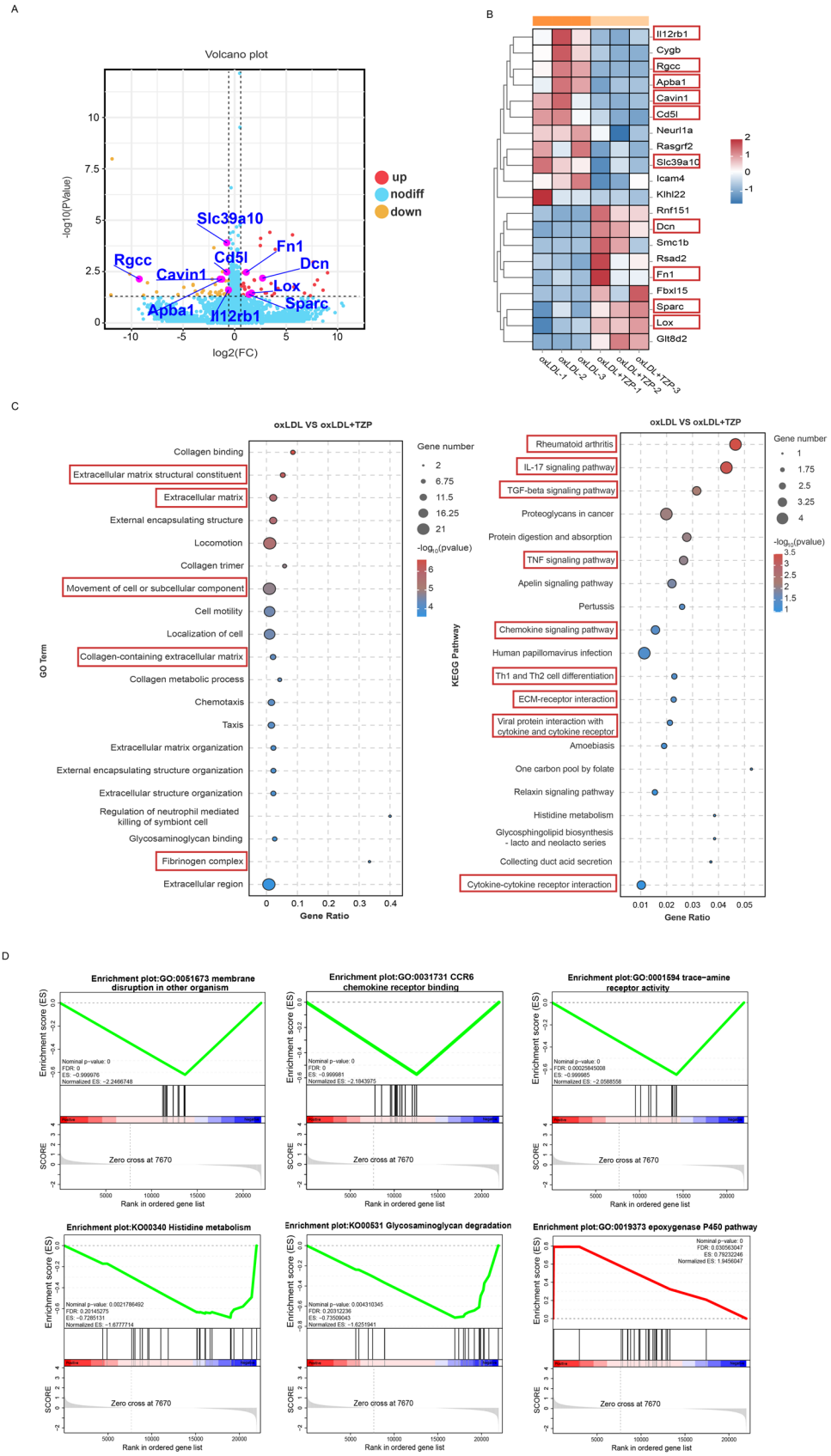

Fig. 5 RNA-Seq analysis of TZP's effects on gene expression in murine RAW264.7 macrophages. **A** Volcano plot showing 38 upregulated and 43 downregulated genes in macrophages treated with TZP in the presence of oxLDL. **B** Heatmap of the top 20 differentially expressed genes, including 10 genes associated with inflammation and atherosclerosis. **C** Selective Kyoto Encyclopedia of Genes and Genomes (KEGG) and Gene Ontology (GO) enrichment analysis highlighting pathways related to inflammation and atherosclerosis. **D** Set enrichment analysis (GSEA) analysis shows TZP downregulated pathways related to glucose and lipid metabolism (green) and upregulated the epoxygenase P450 pathway (red). Fold enrichment ranges from − 0.5 to 0.5, with significance calculated using FDR correction. **FDR-adjusted $p < 0.01$, *FDR-adjusted $p < 0.05$; N = 3

of phospho-IκB/IκB) (Fig. 6A, $p < 0.05$). Importantly, by immunofluorescence assay, we further demonstrated that TZP effectively suppressed oxLDL-induced nuclear translocation of p65 in RAW264.7 macrophages in vitro (Fig S4A & B, $p < 0.05$), and consistently reduced nuclear p65 immunofluorescence intensity in aortic tissues of HF/apo $E^{-/-}$ mice in vivo (Fig. 6B, $p < 0.05$). These results suggest that TZP inhibits oxLDL-induced macrophage activation, suppresses the NFκB inflammatory pathway and restores M1/M2 macrophage homeostasis.

Both GLP-1 and GIP receptors are involved in TZP regulation of M1/M2 macrophage homeostasis

TZP is a dual receptor agonist of GLP-1R and GIPR, and both GLP-1 and GIP agonists have been shown to attenuate the development of atherosclerotic CVDs and regulate macrophage polarization. To elucidate receptor mechanism through which TZP influences macrophage polarization, we determined mRNA expression of GIPR and GLP-1R. The results indicate that both receptors were expressed in murine macrophage, and neither oxLDL nor TZP affect their mRNA expression levels (Fig. 7A, B). To further investigate receptor involvement, murine macrophages were preincubated with either the GLP-1R antagonist or the GIPR antagonist prior to treatment with oxLDL and/or TZP. As anticipated, TZP significantly attenuated the oxLDL-induced upregulation of M1 inflammatory cytokines (TNFα, IL-6, CCL2 and TLR4), and reversed the suppression of M2 macrophage cytokines (IL-10 and Arg-1), preincubation with the GLP-1R antagonist 1 or GIPR antagonist GIP (3-30) NH2 (a potent antagonist of GIPR) partially attenuated TZP's effects on the mRNA expression of these cytokines. However, the combination of GLP-1R antagonist 1 and GIP (3-30) NH2 completely abrogated TZP's effects on M1 cytokines and M2 cytokine expression (Fig. 7C–H, all $p < 0.05$). These results suggest that both GLP-1R and GIPR are essential for TZP-mediated regulation of M1/M2 macrophage homeostasis.

TZP promotes M1/M2 macrophage homeostasis through upregulation of the KLF4/PPARγ pathway in murine macrophages

KLF4 and PPARγ are pivotal regulators of M1/M2 macrophage homeostasis and metabolic profile, both of which significantly influence the progression of atherosclerosis (Han et al. 2023; Zhang et al. 2023). As shown in Fig. 8A and B, oxLDL significantly downregulated the protein expression of KLF4 and PPARγ, an effect that was reversed by TZP treatment. Importantly, this key regulation was corroborated in vivo. Immunofluorescence analysis of aortic tissues from apo $E^{-/-}$ mice fed a high-fat diet revealed a significant reduction in KLF4 expression, which was conversely restored by TZP treatment (Fig. 8C, $p < 0.05$). Bioinformatic analysis revealed multiple binding sites between KLF4 and PPARγ (Fig S5). Furthermore, we treated macrophages with KLF4 inhibitor kenpaullone or PPARγ inhibitor T0070907, kenpaullone attenuated TZP-induced upregulation of KLF4 and PPARγ expression (Fig S6A, $p < 0.05$), whereas T0070907 inhibited TZP-induced upregulation of PPARγ but did not affect KLF4 expression (Fig. 8G, $p < 0.05$), both inhibitors reversed the effects of TZP on oxLDL-mediated expression of M1/M2 macrophage cytokines (Fig S6B, Fig. 8H, all $p < 0.05$). Consistently, KLF4 gene silencing achieved similar effects as the KLF4 inhibitor, with KLF4 protein expression downregulated by approximately 55% (Fig. 8D, $p < 0.05$), confirming the efficiency of silencing. Silencing of KLF4 also suppressed TZP-induced upregulation of PPARγ expression (Fig. 8E, $p < 0.05$) and reversed the effects of TZP on the expression of M1 and M2 cytokines (Fig. 8F, $p < 0.05$). These results suggest that TZP regulates M1/M2 macrophage homeostasis through activation of KLF4/PPARγ pathway.

Discussion

The present study demonstrates that TZP treatment reduces atherosclerotic plaque in atherogenic apo $E^{-/-}$ mice, shifts macrophage polarization from M1 to M2 and improves metabolic profile. In both cultured murine and human macrophages, TZP attenuates oxLDL-induced lipid deposition and foam cell formation, and downregulates CD36. Mechanistically, TZP promotes the M1 to M2 transition through activating the KLF4/PPARγ pathway. These findings suggest that TZP exerts anti-atherosclerotic and CV protective effects.

As a dual agonist of GLP-1R and GIPR, TZP is more effective than GLP-1R agonists in lowering blood glucose and body loss. Unlike traditional glucose-lowering agents, TZP strongly lowers blood glucose level but rarely causes low blood glucose episodes, as it stimulates insulin release in a glucose dependent manner (Del Prato et al. 2021; Wong et al. 2023). Consequently, some investigators regard TZP as a groundbreaking advancement in the treatment of diabetes and obesity (Heise et al. 2022, 2023). Clinical trials have shown that TZP can significantly reduce risk of CVDs in patients with T2D or obesity (Wilson et al. 2020; Garvey et al. 2023; Nicholls et al. 2024). However, since trial participants had underlying metabolic disorders, it remains challenging to distinguish whether the CV protective effects of TZP are solely due to metabolic improvement or involve direct beneficial effect on CV system (Nicholls et al. 2024). Our in vitro results indicate that TZP exerts direct anti-atherosclerotic effects through inhibiting lipid deposition, foam cell formation, and inflammation in oxLDL-treated

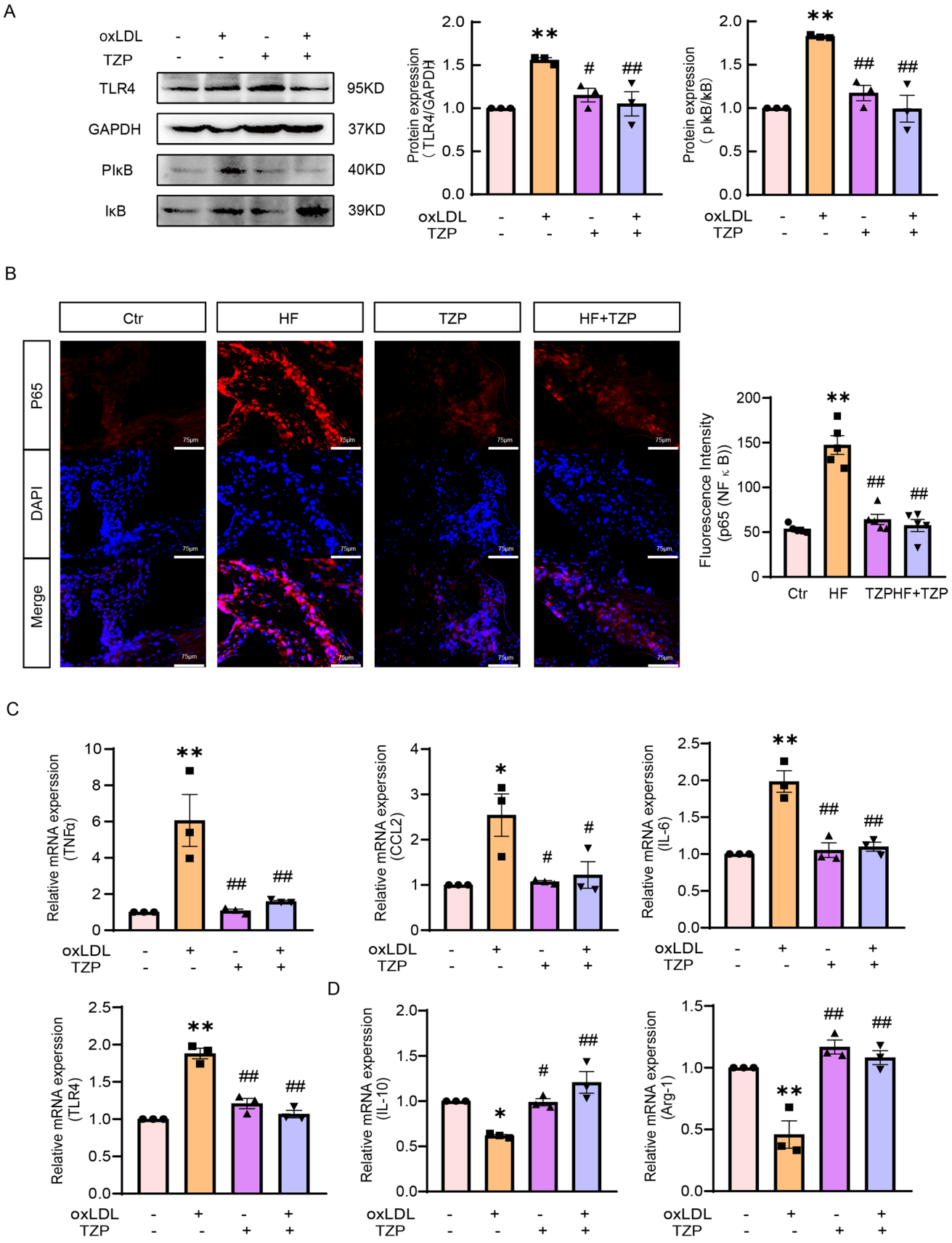
A
oxLDL
TZP
TLR4
GAPDH
PIκB
Iκ B
95KD
37KD
40KD
39KD
Protein expression (TLR4/GAPDH)
Protein expression (pIκB/Iκ B)
B
Ctr
HF
TZP
HF+TZP
P65
DAPI
Merge
75μm
Fluorescence Intensity (p65 (NF κ B))
C
Relative mRNA expression (TNFα)
Relative mRNA expression (CCL2)
Relative mRNA expression (IL-6)
D
Relative mRNA expression (TLR4)
Relative mRNA expression (IL-10)
Relative mRNA expression (Arg-1)

◂**Fig. 6** TZP modulates macrophage inflammatory response and M1/M2 macrophage homeostasis in murine RAW264.7 macrophages. **A** TZP inhibited the protein expression of oxLDL-induced upregulation of Toll-like receptor 4 (TLR4) /nuclear factor kappa B (NFκB, pIκB/Iκ B ratio) pathway, n = 3. **B** Representative immunofluorescence images and their quantitation of p65 (NFκB) nuclear translocation, n = 5. **C** TZP treatment reversed oxLDL-induced increase in M1 pro-inflammatory genes (tumor necrosis factor a (TNFα), C–C motif ligand 2 (CCL2), interleukin (IL)-6, and TLR4), and decrease in expression of M2 anti-inflammatory genes (IL-10 and Arg-1), n = 3. Data are expressed as mean ± SEM. $^{*}p < 0.05$ vs. Ctr group; $^{**}p < 0.01$ vs. Ctr group; $^{\#}p < 0.05$ vs. oxLDL group; $^{\#\#}p < 0.01$ vs. oxLDL group

macrophages. Furthermore, ANCOVA of our in vivo data showed that TZP' s reduction of atherosclerotic lesions remains significant after adjusting for body weight and cholesterol levels. These results suggest that TZP's anti-atherosclerotic effects may involve both metabolic-dependent and metabolic-independent mechanisms.

A key feature of atherosclerosis is the recruitment of macrophages in the arterial wall, where they engulf oxLDL, leading to foam cell formation (Lin et al. 2022; Bao et al. 2024). The accumulation of macrophage foam cells promotes development of early atherosclerotic lesions and sustained plaque growth (Marchio et al. 2019; Ahmed et al. 2023). Plague progression is strongly influenced by cholesterol metabolism within subendothelial macrophages (Ahmed and Myerscough 2024; Skeyni et al. 2024). Intracellular non-esterified cholesterol levels are increased by CD36-mediated oxLDL uptake, while cholesterol efflux is facilitated by ABCA1 and ABCG1 (Yu and Tang 2022; Zhang et al. 2022).

We have previously shown that nicotine accelerates atherosclerosis via upregulating CD36 expression, enhancing lipid uptake and foam cell formation (Zhou et al. 2013). In the present study, we show that TZP downregulates oxLDL-induced CD36 expression while upregulating ABCA1 and ABCG1, which may reduce intracellular lipid accumulation and foam cell formation. We detected both GLP-1 and GIP receptors in murine macrophages. GLP-1R is a G-protein-coupled receptor, and its activation increases intracellular cyclic adenosine monophosphate (cAMP) to induce PKA phosphorylation (Le et al. 2023). Dai et al. showed that GLP-1RA liraglutide inhibits CD36 expression and oxLDL accumulation through GLP-1R/PKA pathway (Dai et al. 2014). Here we found that TZP enhances PKA phosphorylation, and a PKA inhibitor abolished TZP's inhibitory effects on oxLDL-induced macrophage lipid accumulation and foam cell formation. These findings suggest that TZP inhibits oxLDL-induced CD36 expression and lipid deposition primarily through activation of the GLP-1R/PKA pathway.

Atherosclerotic CVDs are considered as a chronic unresolved vascular inflammatory disease initiated by abnormal lipid accumulation in the arterial wall. Macrophages play a pivotal role in driving the inflammatory process (Bäck et al. 2019). M1 macrophages secrete pro-inflammatory mediators that sustain local inflammation, degrade extracellular matrix, and contribute to lesion progression and plaque instability (Luo et al. 2024). In contrast, M2 macrophages express IL-4, IL-10, Arg-1 and TGF-β1, which promote tissue repair and plaque stability (Shapouri-Moghaddam et al. 2018). M2 macrophages are present in many models of regression plaques and involve inflammation resolution and plaque remodeling (Hu et al. 2021). Using RNA-seq and KEGG pathway analysis, we observed that TZP modulates several keys signaling pathways associated with inflammation in oxLDL-pretreated macrophages, such as the TNFα, chemokine, and Th1 and Th2 cell differentiation pathway. TZP inhibited oxLDL-induced M1 markers, while simultaneously enhancing M2 markers. Similar changes in M1/M2 macrophage markers were also found in atherogenic plaques of apo $E^{-/-}$ mice. Specifically, TZP treatment decreases the M1 marker CD86 and iNOS, and increases the M2 marker CD206 and Arg-1, coinciding with significant regression of atherosclerotic lesions. These results suggest that anti-atherosclerotic effects of TZP are mediated at least in part by its anti-inflammatory properties and its ability to restore M1/M2 macrophage homeostasis.

KLF4 has been shown to inhibit proinflammatory gene expression, induces M2 macrophage gene reprogramming, and promote the M1/M2 transition (Qiu et al. 2021). Myeloid specific KLF4 depletion is linked to delayed wound healing and increased susceptibility to diet-induced metabolic disorders, highlighting its role in regulating M1/M2 macrophage homeostasis and metabolic homeostasis (Liao et al. 2011). Furthermore, KLF4 interacts with nuclear receptors such as PPARγ to mediate macrophage polarization (Kapoor et al. 2015; Zhuang et al. 2021; Shao et al. 2023). Shao et al. reported KLF4 binding sites within PPARγ promoter and demonstrated that KLF4 upregulates PPARγ expression (Shao et al. 2023), promoting M2 polarization (Rui et al. 2022).

To investigate the mechanisms by which TZP regulates M1/M2 macrophage homeostasis, we performed bioinformatic analyses to predict interactions between KLF4 and PPARγ. Our bioinformatic analysis identified multiple binding sites between KLF4 and PPARγ. In this study, TZP upregulated both KLF4 and PPARγ in oxLDL-treated macrophage, and pharmacological inhibition of either KLF4 or PPARγ reversed TZP's effects on M1/M2 cytokine expression. Critically, KLF4 gene silencing recapitulated the effects of the pharmacological inhibitor, downregulating both KLF4 and PPARγ expression and abolishing TZP's modulation of macrophage polarization, providing direct genetic evidence for the axis. Moreover, inhibition of KLF4 prevented TZP-induced upregulation of PPARγ, whereas PPARγ inhibition did not affect TZP upregulation of KLF4,

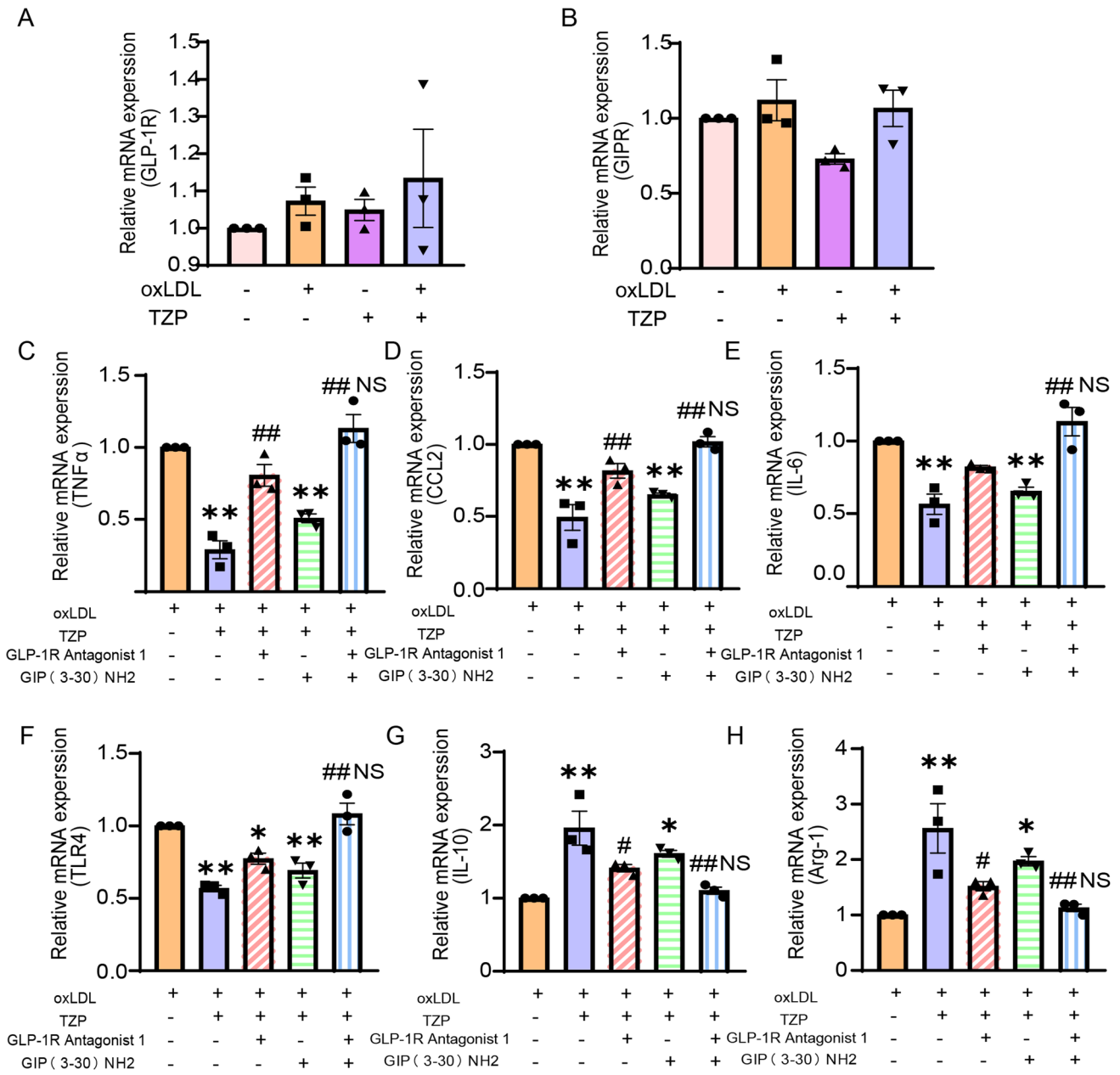

Fig. 7 TZP regulates M1/M2 macrophage homeostasis through GLP-1R and GIPR activation in murine RAW264.7 macrophages. **A** and **B** TZP did not alter mRNA expression of glucagon-like peptide-1 receptor (GLP-1R) or glucose dependent insulinotropic polypeptide receptor (GIPR). **C**–**H** TZP significantly inhibited oxLDL-induced increases in pro-inflammatory cytokines (TNFα, IL-6, CCL2, and TLR4) and prevented reductions in anti-inflammatory cytokines (IL-10 and Arg-1). Data are expressed as mean ± SEM. $^{*}p < 0.05$ vs. oxLDL group; $^{**}p < 0.01$ vs. oxLDL group; $^{\#}p < 0.05$ vs. oxLDL + TZP group; $^{\#\#}p < 0.01$ vs. oxLDL + TZP group; NS: no significant difference compared with oxLDL group. N = 3

placing KLF4 upstream of PPARγ in this pathway. The dependence on dual receptor engagement is confirmed, as combined GLP-1R and GIPR antagonism completely abrogated TZP's regulatory effects. These results suggest that TZP promotes M1/M2 macrophage homeostasis through the upregulation of the KLF4/PPARγ pathway, driven by the activation of both GLP-1 and GIP receptors.

Limitations: Several limitations should be acknowledged. First, a key consideration is whether TZP's anti-atherosclerotic effects are independent of its metabolic benefits. Although ANCOVA suggests partial independence from weight loss and lipid changes, this method has limitations due to variable correlation and sample size. Thus, although in vitro data support direct effects on macrophage

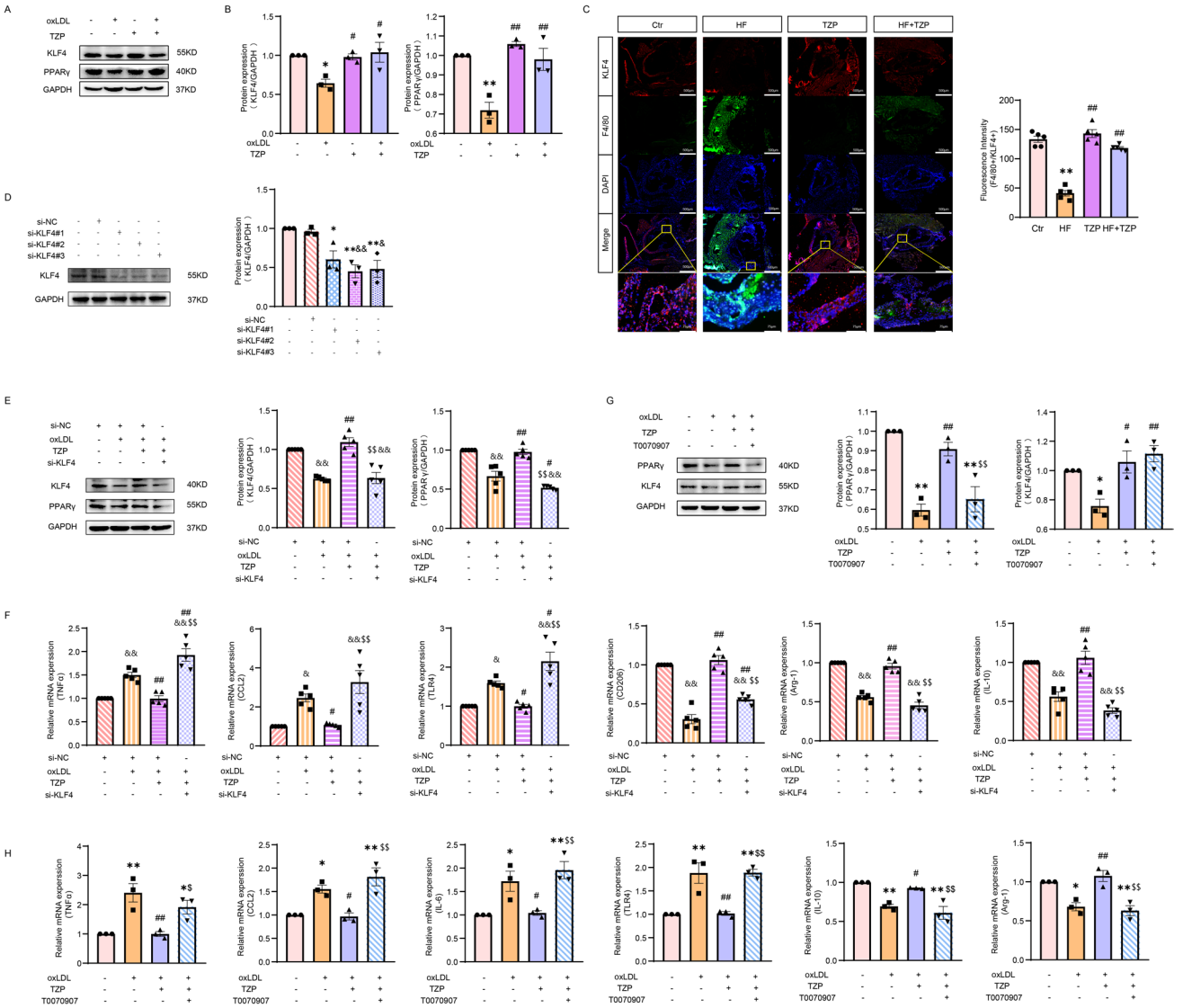

Fig. 8 TZP promotes M1/M2 macrophage homeostasis via kruppel-like factor 4 (KLF4)/peroxisome proliferator-activated receptor (PPAR) γ pathway activation in murine RAW264.7 macrophages. Representative image bands (**A**) of KLF4 and PPARγ and their quantitation (**B**). **C** Representative immunofluorescence images and their quantitation of co-staining for F4/80 and KLF4, n = 3. **D** Effects of three silencing KLF4 gene sequences on the protein expression of KLF4. **E** and **F** Silencing KLF4 gene attenuated TZP upregulation of KLF4 and PPARγ mRNA expression (**E**) and reversed TZP effects on M1 (TNFα, CCL2 & TLR4) and M2 genes (CD206 & Arg-1, IL-10) expression (**F**), n = 5. **G** PPARγ inhibitor T0070907 attenuated TZP upregulation of PPARγ protein expression but did not affect KLF4 expression, and reversed TZP effects on M1/M2 genes mRNA expression (**H**), n = 3. Data are expressed as mean ± SEM. $^{*}p < 0.05$ vs. Ctr group; $^{**}p < 0.01$ vs. Ctr group; $^{\#}p < 0.05$ vs. oxLDL group or si-NC + oxLDL; $^{\#\#}p < 0.01$ vs. oxLDL group or si-NC + oxLDL group; $^{\&}p < 0.05$ vs. si-NC group; $^{\&\&}p < 0.01$ vs. si-NC group; $^{\$}p < 0.05$ vs. oxLDL + TZP group or si-NC + oxLDL + TZP group; $^{\$\$}p < 0.01$ vs. oxLDL + TZP group or si-NC + oxLDL + TZP group

polarization, we cannot definitively conclude that the in vivo anti-atherosclerotic effects are entirely independent of metabolic improvements. Future studies using tissue-specific receptor knockout models or pair-feeding experiments are needed to clarify these mechanisms. Second, while we have added important plaque stability data (necrotic core, fibrous cap) and expanded in vivo immunophenotyping with additional markers (F4/80, iNOS, Arg-1), the sample sizes in the original in vivo and some in vitro experiments, though sufficient to detect the primary reported effects, are modest. This may limit the granularity of subgroup analyses and generalizability. Third, we acknowledge the lack of primary macrophage validation as a limitation. THP-1 cells were chosen for their homogeneity and well-established use in atherosclerosis research (Wang et al. 2024; Cao et al. 2025; Zhang et al. 2025). While this human line supports translational

relevance and enabled our core transcriptomic analyses, it may not fully reflect primary macrophage biology. Confirmatory studies using primary human or murine macrophages are therefore warranted. Fourth, plaque stability depends on multiple factors beyond macrophages. While we focused on macrophage polarization, other elements, such as smooth muscle cell content, fibrous cap thickness and collagen deposition, were not fully assessed. Given that GLP-1 agonists can directly affect vascular smooth muscle and endothelial cells (Ma et al. 2021; McLean et al. 2021; Park et al. 2024; Zhang et al. 2024), TZP may also act through these cell types. Future studies should examine these parameters to better characterize its vascular protective effects. Finally, the in vitro experiments, while informative, involve short-term treatments that may not fully recapitulate the chronic processes of atherosclerotic plaque development in vivo. The in vivo validation of KLF4 expression in plaque macrophages helps bridge this gap, but the inherent differences between model systems remain a consideration.

In conclusion, this study provides first scientific evidence showing that TZP halts atherosclerosis progression in the atherosclerotic apo $E^{-/-}$ mice and suppresses oxLDL-mediated foam cell formation and inflammatory response in macrophages. These effects are mediated at least in part, through the inhibition of CD36-mediated cholesterol uptake and the restoration of M1/M2 macrophage homeostasis via the GLP-1R/GIPR-PKA-KLF4-PPARγ signaling axis. While macrophage modulation represents a key mechanism, future studies should investigate the potential contributions of other cell types to overall atheroprotective effects of TZP. Given the strong association of T2D and obesity with atherosclerotic CVD risk, our findings suggest that TZP could enhance therapeutic strategies for managing diabetes and obesity in individuals at high risk for atherosclerotic CVDs.

Supplementary Information The online version contains supplementary material available at https://doi.org/10.1007/s12272-026-01610-3.

Acknowledgements This work was funded by the National Natural Science Foundation of China (Nos. 81970357, 2019; 82270434, 2022) to Ming-Sheng Zhou, and by Key R&D Project of Liaoning Provincial Department of Science and Technology (2025JH2/101300019), the Research Project of Educational Commission of Liaoning Province (LJ212410164003), and the U35 Outstanding Young Talent Program of Shenyang (RC240612) to Yueyang Liu, and by Key R&D Project of Liaoning Provincial Department of Science and Technology (2024JH2/102500033), Liaoning Provincial Department of Education Research Platform Construction Project (LJ232410164023), Shenyang Science and Technology Bureau Public Health Research and Development Special Project (24-214-3-145) to Junjia Gao. We are indebted to all members who contributed to this work. We are grateful to Dr. Xiaona Hu (Eli Lilly Suzhou Pharmaceutical Company Limited) for her critical review of this manuscript.

Funding The National Natural Science Foundation of China, 81970357, Ming-Sheng Zhou, 82270434, Ming-Sheng Zhou, Key R&D Project of Liaoning Provincial Department of Science and Technology, 2025JH2/101300019, Yueyang Liu, 2024JH2/102500033, Junjia Gao, the Research Project of Educational Commission of Liaoning Province, LJ212410164003, Yueyang Liu,Liaoning Provincial Department of Education Research Platform Construction Project, LJ232410164023, Junjia Gao, Shenyang Science and Technology Bureau Public Health Research and Development Special Project, 24-214-3-145, Junjia Gao.

Data availability The cell RNA-sequencing datasets presented in this study are available in the Gene Expression Omnibus repository (GSE287433).

Declarations

Conflict of interest All authors declare that the work was conducted in the absence of any commercial or financial relationships that could be construed as a potential conflict of interest.

References

Ahmed IU, Myerscough MR (2024) HDL and plaque regression in a multiphase model of early atherosclerosis. Math Biosci. https://doi.org/10.1016/j.mbs.2024.109208

Ahmed IU, Byrne HM, Myerscough MR (2023) Macrophage anti-inflammatory behaviour in a multiphase model of atherosclerotic plaque development. Bull Math Biol 85(5):37. https://doi.org/10.1007/s11538-023-01142-7

Bäck M, Yurdagul A Jr., Tabas I, Öörni K, Kovanen PT (2019) Inflammation and its resolution in atherosclerosis: mediators and therapeutic opportunities. Nat Rev Cardiol 16(7):389–406. https://doi.org/10.1038/s41569-019-0169-2

Bao Q, Zhang B, Zhou L, Yang Q, Mu X, Liu X, Zhang S, Yuan M, Zhang Y, Che J, Wei W, Liu T, Li G, He J (2024) CNP ameliorates macrophage inflammatory response and atherosclerosis. Circ Res 134(8):e72–e91. https://doi.org/10.1161/circresaha.123.324086

Bilal A, Yi F, Gonzalez GR, Ali M, Im K, Ruff CT, Thethi TK, Pratley RE (2024) Effects of newer anti-hyperglycemic agents on cardiovascular outcomes in older adults: systematic review and meta-analysis. J Diabetes Complic 38(8):108783. https://doi.org/10.1016/j.jdiacomp.2024.108783

Bucheit J, Ayers J, Pamulapati L, Browning A, Sisson E (2022) A novel dual incretin agent, Tirzepatide (LY3298176), for the treatment of type 2 diabetes mellitus and cardiometabolic health. J Cardiovasc Pharmacol 80(2):171–179. https://doi.org/10.1097/fjc.0000000000001299

Burnett MS, Durrani S, Stabile E, Saji M, Lee CW, Kinnaird TD, Hoffman EP, Epstein SE (2004) Murine cytomegalovirus infection increases aortic expression of proatherosclerotic genes. Circulation 109(7):893–897. https://doi.org/10.1161/01.Cir.0000112585.47513.45

Cao L, Zhang J, Yu L, Yang W, Qi W, Ren R, Liu Y, Hou Y, Cao Y, Li Q, Wang X, Zhang Z, Li B, Sui W, Zhang Y, Gao C, Zhang C, Zhang M (2025) E3 ubiquitin ligase Listerin regulates macrophage cholesterol efflux and atherosclerosis by targeting ABCA1. J Clin Invest. https://doi.org/10.1172/jci186509

Cersosimo A, Salerno N, Sabatino J, Scatteia A, Bisaccia G, De Rosa S, Dellegrottaglie S, Bucciarelli-Ducci C, Torella D, Leo I (2024) Underlying mechanisms and cardioprotective effects of SGLT2i and GLP-1Ra: insights from cardiovascular magnetic resonance. Cardiovasc Diabetol 23(1):94. https://doi.org/10.1186/s12933-024-02181-7

Chandrasekaran P, Weiskirchen R (2024) The role of obesity in type 2 diabetes mellitus-an overview. Int J Mol Sci. https://doi.org/10.3390/ijms25031882

Chanput W, Mes JJ, Wichers HJ (2014) THP-1 cell line: an in vitro cell model for immune modulation approach. Int Immunopharmacol 23(1):37–45. https://doi.org/10.1016/j.intimp.2014.08.002

Chatzi CA, Basios A, Markozannes G, Ntzani EE, Tsilidis KK, Kazakos K, Agouridis AP, Barkas F, Pappa M, Katsiki N, Rizos EC (2024) Effect of different dietary patterns on cardiometabolic risk factors: an umbrella review of systematic reviews and meta-analyses. Nutrients. https://doi.org/10.3390/nu16223873

Chen GC, Hukportie DN, Liu YJ, Wang HP, Qin LQ, Fan WD, Li FR, Wu XB (2024) Microvascular disease, cardiovascular health, and risk of coronary heart disease in type 2 diabetes: a UK Biobank study. J Clin Endocrinol Metab 109(9):2335–2342. https://doi.org/10.1210/clinem/dgae100

Dai Y, Dai D, Wang X, Ding Z, Li C, Mehta JL (2014) GLP-1 agonists inhibit ox-LDL uptake in macrophages by activating protein kinase A. J Cardiovasc Pharmacol 64(1):47–52. https://doi.org/10.1097/fjc.0000000000000087

Dardano A, Bianchi C, Garofolo M, Del Prato S (2024) The current landscape for diabetes treatment: preventing diabetes-associated CV risk. Atherosclerosis. https://doi.org/10.1016/j.atherosclerosis.2024.117560

Del Prato S, Kahn SE, Pavo I, Weerakkody GJ, Yang Z, Doupis J, Aizenberg D, Wynne AG, Riesmeyer JS, Heine RJ, Wiese RJ (2021) Tirzepatide versus insulin glargine in type 2 diabetes and increased cardiovascular risk (SURPASS-4): a randomised, open-label, parallel-group, multicentre, phase 3 trial. Lancet 398(10313):1811–1824. https://doi.org/10.1016/s0140-6736(21)02188-7

Dinsmore TC, Liu J, Miao J, Ünsal Ö, Sürmeli D, Beinborn M, Lin YS, Kumar K (2024) Potent and protease resistant azapeptide agonists of the GLP-1 and GIP receptors. Angew Chem Int Ed Engl 63(49):e202410237. https://doi.org/10.1002/anie.202410237

Garvey WT, Frias JP, Jastreboff AM, Le Roux CW, Sattar N, Aizenberg D, Mao H, Zhang S, Ahmad NN, Bunck MC, Benabbad I, Zhang XM (2023) Tirzepatide once weekly for the treatment of obesity in people with type 2 diabetes (SURMOUNT-2): a double-blind, randomised, multicentre, placebo-controlled, phase 3 trial. Lancet 402(10402):613–626. https://doi.org/10.1016/s0140-6736(23)01200-x

Gianopoulos I, Mantzoros CS, Daskalopoulou SS (2025) Adiponectin and adiponectin receptors in atherosclerosis. Endocr Rev 46(1):1–25. https://doi.org/10.1210/endrev/bnae021

Gilbert MP, Pratley RE (2020) GLP-1 analogs and DPP-4 inhibitors in type 2 diabetes therapy: review of head-to-head clinical trials. Front Endocrinol. https://doi.org/10.3389/fendo.2020.00178

Groh L, Keating ST, Joosten LA, Netea MG, Riksen NP (2018) Monocyte and macrophage immunometabolism in atherosclerosis. Semin Immunopathol 40(2):203–214. https://doi.org/10.1007/s00281-017-0656-7

Hammoud R, Kaur KD, Koehler JA, Baggio LL, Wong CK, Advani KE, Yusta B, Efimova I, Gribble FM, Reimann F, Fishman S, Varol C, Drucker DJ (2024) Glucose-dependent insulinotropic polypeptide receptor signaling alleviates gut inflammation in mice. JCI Insight. https://doi.org/10.1172/jci.insight.174825

Han Z, Hu H, Yin M, Lin Y, Yan Y, Han P, Liu B, Jing B (2023) HOXA1 participates in VSMC-to-macrophage-like cell transformation via regulation of NF-κB p65 and KLF4: a potential mechanism of atherosclerosis pathogenesis. Mol Med 29(1):104. https://doi.org/10.1186/s10020-023-00685-8

Hankosky ER, Wang H, Neff LM, Kan H, Wang F, Ahmad NN, Griffin R, Stefanski A, Garvey WT (2024) Tirzepatide reduces the predicted risk of atherosclerotic cardiovascular disease and improves cardiometabolic risk factors in adults with obesity or overweight: SURMOUNT-1 post hoc analysis. Diabetes Obes Metab 26(1):319–328. https://doi.org/10.1111/dom.15318

Heise T, Mari A, Devries JH, Urva S, Li J, Pratt EJ, Coskun T, Thomas MK, Mather KJ, Haupt A, Milicevic Z (2022) Effects of subcutaneous tirzepatide versus placebo or semaglutide on pancreatic islet function and insulin sensitivity in adults with type 2 diabetes: a multicentre, randomised, double-blind, parallel-arm, phase 1 clinical trial. Lancet Diabetes Endocrinol 10(6):418–429. https://doi.org/10.1016/s2213-8587(22)00085-7

Heise T, Devries JH, Urva S, Li J, Pratt EJ, Thomas MK, Mather KJ, Karanikas CA, Dunn J, Haupt A, Milicevic Z, Coskun T (2023) Tirzepatide reduces appetite, energy intake, and fat mass in people with type 2 diabetes. Diabetes Care 46(5):998–1004. https://doi.org/10.2337/dc22-1710

Hu D, Wang Z, Wang Y, Liang C (2021) Targeting macrophages in atherosclerosis. Curr Pharm Biotechnol 22(15):2008–2018. https://doi.org/10.2174/1389201022666210122142233

Huang Y, Mo H, Yang J, Gao L, Tao T, Shu Q, Guo W, Zhao Y, Lyu J, Wang Q, Guo J, Zhai H, Zhu L, Chen H, Xu G (2024) Mechanoregulation of GLP-1 production by Piezo1 in intestinal L cells. Elife. https://doi.org/10.7554/eLife.97854

Kapoor N, Niu J, Saad Y, Kumar S, Sirakova T, Becerra E, Li X, Kolattukudy PE (2015) Transcription factors STAT6 and KLF4 implement macrophage polarization via the dual catalytic powers of MCPIP. J Immunol 194(12):6011–6023. https://doi.org/10.4049/jimmunol.1402797

Kassi E, Kyrou I, Randeva HS (2023) Atherosclerotic and cardio-metabolic diseases: from molecular basis to therapeutic advances. Int J Mol Sci. https://doi.org/10.3390/ijms24119737

Katogiannis K, Thymis J, Kousathana F, Pavlidis G, Korakas E, Kountouri A, Balampanis K, Prentza V, Kostelli G, Michalopoulou H, Tsilivarakis D, Lambadiari V, Ikonomidis I (2024) Effects of liraglutide, empagliflozin and their combination on left atrial strain and arterial function. Medicina 60(3):395. https://doi.org/10.3390/medicina60030395

Kufazvinei TTJ, Chai J, Boden KA, Channon KM, Choudhury RP (2024) Emerging opportunities to target inflammation: myocardial infarction and type 2 diabetes. Cardiovasc Res 120(11):1241–1252. https://doi.org/10.1093/cvr/cvae142

Kunutsor SK, Seidu BS, Seidu S (2024) Cardiovascular effectiveness of newer glucose-lowering agents, with and without baseline lipid-lowering therapy in type 2 diabetes: a systematic meta-analysis of cardiovascular outcome trials and real-world evidence. Prim Care Diabetes 18(6):589–598. https://doi.org/10.1016/j.pcd.2024.09.007

Kwan TW, Wong SS, Hong Y, Kanaya AM, Khan SS, Hayman LL, Shah SH, Welty FK, Deedwania PC, Khaliq A, Palaniappan LP (2023) Epidemiology of diabetes and atherosclerotic cardiovascular disease among Asian American adults: implications, management, and future directions: a scientific statement from the American Heart Association. Circulation 148(1):74–94. https://doi.org/10.1161/cir.0000000000001145

Lalić NM, Jotić A, Lukić L, Miličić T, Maćešić M, Stanarčić Gajović J, Stoiljković M, Milovančević M, Rafailović Cvetković D, Lalić K (2024) Glucose lowering drug or strategy dependent impact of weight reduction on the prevention of CVD outcomes in type 2 diabetes: a systematic review of CVOTs. Diabetes Res Clin Pract. https://doi.org/10.1016/j.diabres.2024.111816

Le TDV, Liu D, Besing GK, Raghavan R, Ellis BJ, Ceddia RP, Collins S, Ayala JE (2023) Glucagon-like peptide-1 receptor activation stimulates PKA-mediated phosphorylation of Raptor and this contributes to the weight loss effect of liraglutide. Elife. https://doi.org/10.7554/eLife.80944

Liao X, Sharma N, Kapadia F, Zhou G, Lu Y, Hong H, Paruchuri K, Mahabeleshwar GH, Dalmas E, Venteclef N, Flask CA, Kim J, Doreian BW, Lu KQ, Kaestner KH, Hamik A, Clément K, Jain MK (2011) Krüppel-like factor 4 regulates macrophage

polarization. J Clin Invest 121(7):2736–2749. https://doi.org/10.1172/jci45444

Lin HP, Singla B, Ahn W, Ghoshal P, Blahove M, Cherian-Shaw M, Chen A, Haller A, Hui DY, Dong K, Zhou J, White J, Stranahan AM, Jasztal A, Lucas R, Stansfield BK, Fulton D, Chlopicki S, Csányi G (2022) Receptor-independent fluid-phase macropinocytosis promotes arterial foam cell formation and atherosclerosis. Sci Transl Med 14(663):eadd2376. https://doi.org/10.1126/scitranslmed.add2376

Liu L, Guo H, Song A, Huang J, Zhang Y, Jin S, Li S, Zhang L, Yang C, Yang P (2020) Progranulin inhibits LPS-induced macrophage M1 polarization via NF-κB and MAPK pathways. BMC Immunol 21(1):32. https://doi.org/10.1186/s12865-020-00355-y

Luo M, Zhao F, Cheng H, Su M, Wang Y (2024) Macrophage polarization: an important role in inflammatory diseases. Front Immunol 15:1352946. https://doi.org/10.3389/fimmu.2024.1352946

Ma X, Liu Z, Ilyas I, Little PJ, Kamato D, Sahebka A, Chen Z, Luo S, Zheng X, Weng J, Xu S (2021) GLP-1 receptor agonists (GLP-1RAs): cardiovascular actions and therapeutic potential. Int J Biol Sci 17(8):2050–2068. https://doi.org/10.7150/ijbs.59965

Marchio P, Guerra-Ojeda S, Vila JM, Aldasoro M, Victor VM, Mauricio MD (2019) Targeting early atherosclerosis: a focus on oxidative stress and inflammation. Oxid Med Cell Longev 2019:8563845. https://doi.org/10.1155/2019/8563845

Mather KJ, Mari A, Heise T, Devries JH, Hua M, Urva S, Coskun T, Haupt A, Heine RJ, Pratt E, Thomas MK, Milicevic Z (2024) Effects of tirzepatide vs semaglutide on β-cell function, insulin sensitivity, and glucose control during a meal test. J Clin Endocrinol Metab 109(12):3046–3054. https://doi.org/10.1210/clinem/dgae319

Mclean BA, Wong CK, Kaur KD, Seeley RJ, Drucker DJ (2021) Differential importance of endothelial and hematopoietic cell GLP-1Rs for cardiometabolic versus hepatic actions of semaglutide. JCI Insight 6(22):e153732. https://doi.org/10.1172/jci.insight.153732

Nicholls SJ, Bhatt DL, Buse JB, Prato SD, Kahn SE, Lincoff AM, Mcguire DK, Nauck MA, Nissen SE, Sattar N, Zinman B, Zoungas S, Basile J, Bartee A, Miller D, Nishiyama H, Pavo I, Weerakkody G, Wiese RJ, D'alessio D (2024) Comparison of tirzepatide and dulaglutide on major adverse cardiovascular events in participants with type 2 diabetes and atherosclerotic cardiovascular disease: SURPASS-CVOT design and baseline characteristics. Am Heart J. https://doi.org/10.1016/j.ahj.2023.09.007

Ormazabal V, Nair S, Elfeky O, Aguayo C, Salomon C, Zuñiga FA (2018) Association between insulin resistance and the development of cardiovascular disease. Cardiovasc Diabetol 17(1):122. https://doi.org/10.1186/s12933-018-0762-4

Park JJ (2021) Epidemiology, pathophysiology, diagnosis and treatment of heart failure in diabetes. Diabetes Metab J 45(2):146–157. https://doi.org/10.4093/dmj.2020.0282

Park B, Bakbak E, Teoh H, Krishnaraj A, Dennis F, Quan A, Rotstein OD, Butler J, Hess DA, Verma S (2024) GLP-1 receptor agonists and atherosclerosis protection: the vascular endothelium takes center stage. Am J Physiol Heart Circ Physiol 326(5):H1159-h1176. https://doi.org/10.1152/ajpheart.00574.2023

Paul S, Chhatar S, Mishra A, Lal G (2019) Natural killer t cell activation increases iNOS^{+}CD206^{-} M1 macrophage and controls the growth of solid tumor. J Immunother Cancer 7(1):208. https://doi.org/10.1186/s40425-019-0697-7

Qiu Y, Xu J, Yang L, Zhao G, Ding J, Chen Q, Zhang N, Yang R, Wang J, Li S, Zhang L (2021) MiR-375 silencing attenuates pro-inflammatory macrophage response and foam cell formation by targeting KLF4. Exp Cell Res 400(1):112507. https://doi.org/10.1016/j.yexcr.2021.112507

Regmi A, Aihara E, Christe ME, Varga G, Beyer TP, Ruan X, Beebe E, O'Farrell LS, Bellinger MA, Austin AK, Lin Y, Hu H, Konkol DL, Wojnicki S, Holland AK, Friedrich JL, Brown RA, Estelle AS, Badger HS, Gaidosh GS, Kooijman S, Rensen PCN, Coskun T, Thomas MK, Roell W (2024) Tirzepatide modulates the regulation of adipocyte nutrient metabolism through long-acting activation of the GIP receptor. Cell Metab 36(7):1534–1549. https://doi.org/10.1016/j.cmet.2024.05.010

Rui Y, Han X, Jiang A, Hu J, Li M, Liu B, Qian F, Huang L (2022) Eucalyptol prevents bleomycin-induced pulmonary fibrosis and M2 macrophage polarization. Eur J Pharmacol 931:175184. https://doi.org/10.1016/j.ejphar.2022.175184

Shao X, Xu P, Ji L, Wu B, Zhan Y, Zhuang X, Ou Y, Hua F, Sun L, Li F, Wang X, Chen H, Cheng Y (2023) Low-dose decitabine promotes M2 macrophage polarization in patients with primary immune thrombocytopenia via enhancing KLF4 binding to PPARγ promoter. Clin Transl Med 13(7):e1344. https://doi.org/10.1002/ctm2.1344

Shapouri-Moghaddam A, Mohammadian S, Vazini H, Taghadosi M, Esmaeili SA, Mardani F, Seifi B, Mohammadi A, Afshari JT, Sahebkar A (2018) Macrophage plasticity, polarization, and function in health and disease. J Cell Physiol 233(9):6425–6440. https://doi.org/10.1002/jcp.26429

Skeyni A, Pradignac A, Matz RL, Terrand J, Boucher P (2024) Cholesterol trafficking, lysosomal function, and atherosclerosis. Am J Physiol Cell Physiol 326(2):C473-c486. https://doi.org/10.1152/ajpcell.00415.2023

Van Sloten TT, Sedaghat S, Carnethon MR, Launer LJ, Stehouwer CDA (2020) Cerebral microvascular complications of type 2 diabetes: stroke, cognitive dysfunction, and depression. Lancet Diabetes Endocrinol 8(4):325–336. https://doi.org/10.1016/s2213-8587(19)30405-x

Wang B, Tang X, Yao L, Wang Y, Chen Z, Li M, Wu N, Wu D, Dai X, Jiang H, Ai D (2022) Disruption of USP9X in macrophages promotes foam cell formation and atherosclerosis. J Clin Invest. https://doi.org/10.1172/jci154217

Wang A, Guan B, Yu L, Liu Q, Hou Y, Li Z, Sun D, Xu H (2024) Palmatine protects against atherosclerosis by gut microbiota and phenylalanine metabolism. Pharmacol Res 209:107413. https://doi.org/10.1016/j.phrs.2024.107413

Wilson JM, Nikooienejad A, Robins DA, Roell WC, Riesmeyer JS, Haupt A, Duffin KL, Taskinen MR, Ruotolo G (2020) The dual glucose-dependent insulinotropic peptide and glucagon-like peptide-1 receptor agonist, tirzepatide, improves lipoprotein biomarkers associated with insulin resistance and cardiovascular risk in patients with type 2 diabetes. Diabetes Obes Metab 22(12):2451–2459. https://doi.org/10.1111/dom.14174

Wong E, Cope R, Dima L, Nguyen T (2023) Tirzepatide: a dual glucose-dependent insulinotropic polypeptide and glucagon-like Peptide-1 agonist for the management of Type 2 diabetes mellitus. Am J Ther 30(1):e26–e35. https://doi.org/10.1097/mjt.0000000000001588

Yu XH, Tang CK (2022) ABCA1, ABCG1, and cholesterol homeostasis. Adv Exp Med Biol. https://doi.org/10.1007/978-981-19-1592-5_7

Zhang Y, Dong D, Xu X, He H, Zhu Y, Lei T, Ou H (2022) Oxidized high-density lipoprotein promotes CD36 palmitoylation and increases lipid uptake in macrophages. J Biol Chem 298(6):102000. https://doi.org/10.1016/j.jbc.2022.102000

Zhang M, Hou L, Tang W, Lei W, Lin H, Wang Y, Long H, Lin S, Chen Z, Wang G, Zhao G (2023) Oridonin attenuates atherosclerosis by inhibiting foam macrophage formation and inflammation through FABP4/PPARγ signalling. J Cell Mol Med 27(24):4155–4170. https://doi.org/10.1111/jcmm.18000

Zhang K, Li R, Matniyaz Y, Yu R, Pan J, Liu W, Wang D (2024) Liraglutide attenuates angiotensin II-induced aortic dissection and aortic aneurysm via inhibiting M1 macrophage polarization

in APOE$^{/}$ mice. Biochem Pharmacol 223:116170. https://doi.org/10.1016/j.bcp.2024.116170

Zhang Y, Yan C, Dong Y, Zhao J, Yang X, Deng Y, Su L, Yin J, Zhang Y, Sun F, Feng Y (2025) ANGPTL3 accelerates atherosclerotic progression via direct regulation of M1 macrophage activation in plaque. J Adv Res. https://doi.org/10.1016/j.jare.2024.05.011

Zhou MS, Chadipiralla K, Mendez AJ, Jaimes EA, Silverstein RL, Webster K, Raij L (2013) Nicotine potentiates proatherogenic effects of oxLDL by stimulating and upregulating macrophage CD36 signaling. Am J Physiol Heart Circ Physiol 305(4):H563–H574. https://doi.org/10.1152/ajpheart.00042.2013

Zhuang H, Han S, Lu L, Reeves WH (2021) Myxomavirus serpin alters macrophage function and prevents diffuse alveolar hemorrhage in pristane-induced lupus. Clin Immunol 229:108764. https://doi.org/10.1016/j.clim.2021.108764